

Original Article

Cite this article: Köhler S, Duschl F, Fazlikhani H, Koehn D, Stephan T, and Stollhofen H (2023) Reconstruction of cyclic Mesozoic–Cenozoic stress development in SE Germany using fault-slip and stylolite inversion. *Geological Magazine* **159**: 2323–2345. <https://doi.org/10.1017/S0016756822000656>

Received: 9 November 2021

Revised: 10 June 2022

Accepted: 11 June 2022

First published online: 19 August 2022







Keywords:

palaeostress; stylolites; Alpine Orogeny; tectonic cycles; stress inversion; basin inversion

Author for correspondence:

Saskia Köhler, Email: saskia.koehler@fau.de

Reconstruction of cyclic Mesozoic–Cenozoic stress development in SE Germany using fault-slip and stylolite inversion

Saskia Köhler¹ , Florian Duschl^{1,2} , Hamed Fazlikhani¹ , Daniel Koehn¹ , Tobias Stephan^{1,3}  and Harald Stollhofen¹ 

¹GeoZentrum Nordbayern, Friedrich-Alexander Universität (FAU) Erlangen-Nürnberg, Schlossgarten 5, Erlangen 91054, Germany; ²Technical University of Munich, Geothermal Technologies, Arcisstrasse 21, Munich 80333, Germany and ³Department of Geoscience, University of Calgary, Calgary, Alberta T2N 1N4, Canada

Abstract

The Franconian Platform of SE Germany and the underlying Permian and Triassic rocks that developed from latest Permian to Triassic time were affected by multiple compressional and extensional events that created a complex fracture, fault and stylolite network. We reconstructed the spatio-temporal variations of post-Triassic palaeostress fields in the Franconian Platform and Triassic strata using fault-slip and tectonic stylolite inversion. Our highly resolved stress inversion enables us to demonstrate a cyclic stress evolution from the stress regime of normal faulting to thrusting, strike-slip and back to normal faulting. Five main stress fields correlating with two stress cycles are determined for Late Jurassic to Cenozoic time. The first cycle consists of: (SF1) an initially NE–SW-directed horizontal extension during Late Jurassic to Early Cretaceous time; (SF2) NNE–SSW-directed horizontal compression with an early set of tectonic stylolites prior to the development of reverse and thrust faults; and (SF3) a strike-slip-dominated setting with (N)NE–(S)SW horizontal compression representing a first relaxation. The second cycle comprises (SF4) NW–SE-directed horizontal extension during Oligocene–Miocene time; and (SF5) a second strike-slip-dominated regime with WNW–ESE to NW–SE horizontal compression during the Alpine shortening, creating the youngest set of tectonic stylolites. In addition, we consider the transitional stages between thrusting and a strike-slip regime as a snapshot in the process of intraplate tectonics.

1. Introduction

A fold-and-thrust belt generally comprises thrust-folded sedimentary sequences and can include basement and older faults (Twiss & Moores, 1992). The structural life cycle of a typical fold-and-thrust belt is characterized by a series of deformational phases starting with the burial of sedimentary rocks under extension, followed by the inversion of the former basin in a sequence of strike-slip and thrusting (Tavani *et al.* 2015; Ferrill *et al.* 2021). Initial relaxation is represented by another strike-slip regime, followed by the final relaxation due to decreasing shortening and increasing extension (Ferrill *et al.* 2021). The temporal evolution of a fold-and-thrust belt, in particular the changes between the deformation phases and stress regimes, is essential to understand the associated tectonic architecture and stress development in the hinterland.

Intraplate fold-and-thrust belts result from localized shortening of sedimentary basins distal from the plate boundary, such as the Tajik basins (e.g. Stübner *et al.* 2013) or the Sevier and Bighorn basins in the USA, and in North America (e.g. van der Pluijm *et al.* 1997; Beaudoin & Lacombe, 2018). A prominent example of intraplate shortening is the European Alpine Foreland (e.g. Ziegler *et al.* 1995; Cloetingh & van Wees, 2005). In this region, several palaeostress analyses reveal multiple alternating and overlapping phases of contractional and extensional deformation during the Mesozoic and Cenozoic times (Bergerat, 1987; Blés *et al.* 1989; Hibschi *et al.* 1995; Peterek *et al.* 1996; Kley & Voigt, 2008; Sippel *et al.* 2009, 2010; Coubal *et al.* 2015; Navabpour *et al.* 2017). Such phases of deformation were linked to the opening of the Neotethys during the Permian to Early Mesozoic time, the onset of Atlantic rifting, and the development of an active margin between the European and African plates (Scheck-Wenderoth *et al.* 2008).

Previous palaeostress reconstructions from the Franconian Platform in southern Germany, based on fault-slip analysis and subordinate stylolite stress inversion, reveal regionally and temporally differing stress fields (Peterek *et al.* 1996, 1997). Moreover, geo- and thermochronological studies indicate the existence of several intervening extensional phases during the Late Cretaceous and Cenozoic convergence between Europe and Africa (Abratis *et al.* 2007; von Eynatten *et al.* 2019, 2021). So far, however, the stress field evolution was not correlated with

© The Author(s), 2022. Published by Cambridge University Press. This is an Open Access article, distributed under the terms of the Creative Commons Attribution licence (<http://creativecommons.org/licenses/by/4.0/>), which permits unrestricted re-use, distribution and reproduction, provided the original article is properly cited.



neighbouring areas nor was it placed in the context of major tectonic events affecting the area, e.g. Late Cretaceous inversion and subsequent Alpine shortening (Bergerat & Geysant, 1982; Peterek *et al.* 1996, 1997).

We aim to extend the interpretation of the tectonic history of Central Europe by increasing the temporal and spatial resolution of the palaeostress evolution in the Mesozoic sequences west of the Franconian fault zone compared to previous work by using fault-slip and stylolite stress inversion.

With our work we contribute to the understanding of the stress development and the development of intra-continental areas in close vicinity to mountain chains. In addition, the high local resolution allows for identifying local stress perturbations in predicted stress fields.

2. Geological setting

The Franconian Platform is situated immediately west of the Bohemian Massif (Fig. 1c) and consists of Mesozoic and Cenozoic sedimentary rocks (Freudenberger & Schwerd, 1996). The rocks of the Variscides (Kossmat, 1927) exposed in the Bohemian Massif are buried in the west beneath the Kraichgau Basin fill and the sediments of the Franconian Platform (Paul & Schröder, 2012; Sittig, 2012; Kämmlin *et al.* 2020; Fazlikhani *et al.* 2022). The structural framework at the eastern basin margin is dominated by a NW–SE-striking fault network, the most prominent elements of which are the Franconian and the Eisfeld–Kulmbach fault zones.

The Variscan basement was affected by Late Variscan NNW–SSE shortening resulting in final folding and the activation of NE–SW- and NW–SE-striking sinistral and dextral strike-slip systems (Kroner *et al.* 2007; Büttner, 2012; Stephan *et al.* 2016). Beginning in the latest Carboniferous, predominant extensional tectonics associated with the incipient break-up of Pangaea (Kroner & Romer, 2013) led to fault reactivation and formation of structures that follow the strike of pre-existent basin structures and faults (Peterek *et al.* 1997). These latest to post-Variscan tectonics initiated subsidence and the development of WNW- and N- to NE-striking graben systems in Central Europe (Scheck-Wenderoth *et al.* 2008).

Triassic deposits in the study area are fairly tabular with local lateral thickness changes and limited faulting, indicating continuous regional tectonic quiescence (Fig. 1d; Fazlikhani *et al.* 2022).

During the Late Jurassic to Early Cretaceous time (75–55 Ma) the study area was dominated by regional uplift and subsidence to the west of the Bohemian Massif associated with NE–SW-directed horizontal extension (Peterek *et al.* 1996, 1997; Scheck-Wenderoth *et al.* 2008; von Eynatten *et al.* 2021). Late Jurassic sedimentation is controlled by the transgression of the Tethys Ocean from the south which produced a massive carbonate platform (Meyer & Schmidt-Kaler, 1990). For most parts of Central Europe, including large parts of SE Germany, normal faults bounding NW–SE striking graben systems were active at that time, e.g. grabens of the South German Basin (Peterek *et al.* 1997; Zulauf & Duyster, 1997; Walter, 2007; Kley & Voigt, 2008; Scheck-Wenderoth *et al.* 2008; Sippel *et al.* 2009; Navabpour *et al.* 2017). According to Navabpour *et al.* (2017) this phase of normal faulting is also recorded in Middle Triassic rocks in the Thuringian Basin towards the north.

During Late Cretaceous time, the convergence between Iberia–Africa and Europe caused widespread uplift in Central Europe (Kley & Voigt, 2008; Dielforder *et al.* 2019). Increasing thicknesses

and coarsening trends of conglomerates in Lower and Upper Cretaceous units from the (S)W towards (N)E (Hejl *et al.* 1997; Tanner *et al.* 1998; Niebuhr *et al.* 2014) suggest the reactivation of ten to hundreds of kilometres long NW-striking faults (e.g. Pfahl shear zone, Franconian fault zone, Danube shear zone; Schröder, 1987; Scheck-Wenderoth *et al.* 2008). This intraplate compression, together with lithospheric buckling, i.e. long wavelengths and low amplitudes, affected large parts of the South German Basin (Scheck-Wenderoth *et al.* 2008). It lasted until Palaeocene time (Voigt *et al.* 2021) and was accompanied by the inversion of pre-existing grabens (Schröder, 1987; Scheck-Wenderoth *et al.* 2008) and reactivation of NW-trending fault zones (Peterek *et al.* 1997; Tanner *et al.* 1998). Comparing the timing of tectonic activity in individual regions reveals that the inferred relative-chronological order of reverse and strike-slip faulting suggested for Late Cretaceous time does not coincide, even across directly neighbouring areas (Bergerat & Geysant, 1982; Peterek *et al.* 1996; Sippel *et al.* 2009; Navabpour *et al.* 2017). From the Franconian Platform, for instance, the relative order of thrusting and strike-slip faulting was not possible so far (Peterek *et al.* 1996) while in the Thuringian Basin farther north, strike-slip movements occurred prior to reverse faulting (Navabpour *et al.* 2017).

From Eocene to late Oligocene time there is no direct structural evidence for tectonic activity (Peterek *et al.* 1997). In Oligocene and early Miocene time, volcanism penetrates the Franconian Platform marked by the 19–24 Ma Oberpfalz volcanics to the east (c. 50 km to the city of Bayreuth) (Todt & Lippolt, 1975) and the c. 31 Ma ultramafic Oberleinleiter volcanics ESE (c. 15 km from the city of Bamberg) (Hofbauer, 2008). Since Eocene time, contemporaneously forming grabens of the European Cenozoic Rift System (ECRIS) record a variety of extensional directions with the WNW–ESE-directed opening of the NNE–SSW-striking Upper Rhine Graben providing the most prominent example (Ziegler, 1992). The NE–SW-striking Eger Rift, however, initially opened NNE–SSW to N–S and then became overprinted by later NW–SE opening (Ziegler, 1992; Schröder *et al.* 1997; Abratis *et al.* 2007; Rajchl *et al.* 2009).

Collision between Europe and Adria–Africa culminated in the formation of the European Alps and triggered intraplate shortening to the north (Rosenbaum *et al.* 2002; Scheck-Wenderoth *et al.* 2008; Glotzbach *et al.* 2010). Dèzes *et al.* (2004) propose a correlation of contemporaneous volcanism, the opening of the European Cenozoic Rift System (ECRIS) and N-directed shortening induced by the Alpine Orogeny. In the North Alpine Foreland Basin, the increasing tectonic load of the northward-propagating Alpine thrusts led to subsidence and bulging of the lower plate associated with a normal faulting regime in the extensional area of the bulge (von Hartmann *et al.* 2016). Thus the Franconian Platform was affected by the opening of the Eger Rift towards the east and the Alpine collision towards the south (Adamovič & Coubal, 1999; Reicherter *et al.* 2008; Rajchl *et al.* 2009). Towards the east of our study area, historical and recent earthquakes register ongoing seismic activity (Wilde-Piörko *et al.* 2006), and mofettes and thermal springs imply deep-reaching zones of structural permeability extending from the Eger Rift across the Franconian fault zone (e.g. Heinicke *et al.* 2019). In the research borehole Lindau 1, near Bayreuth (Fig. 1a), the mean direction of the maximum present-day horizontal stress, derived from borehole breakouts and from hydraulic stimulation experiments, is 135° and 138° (NW–SE), respectively (Röckel & Wonik, 2006). This differs only slightly from results of

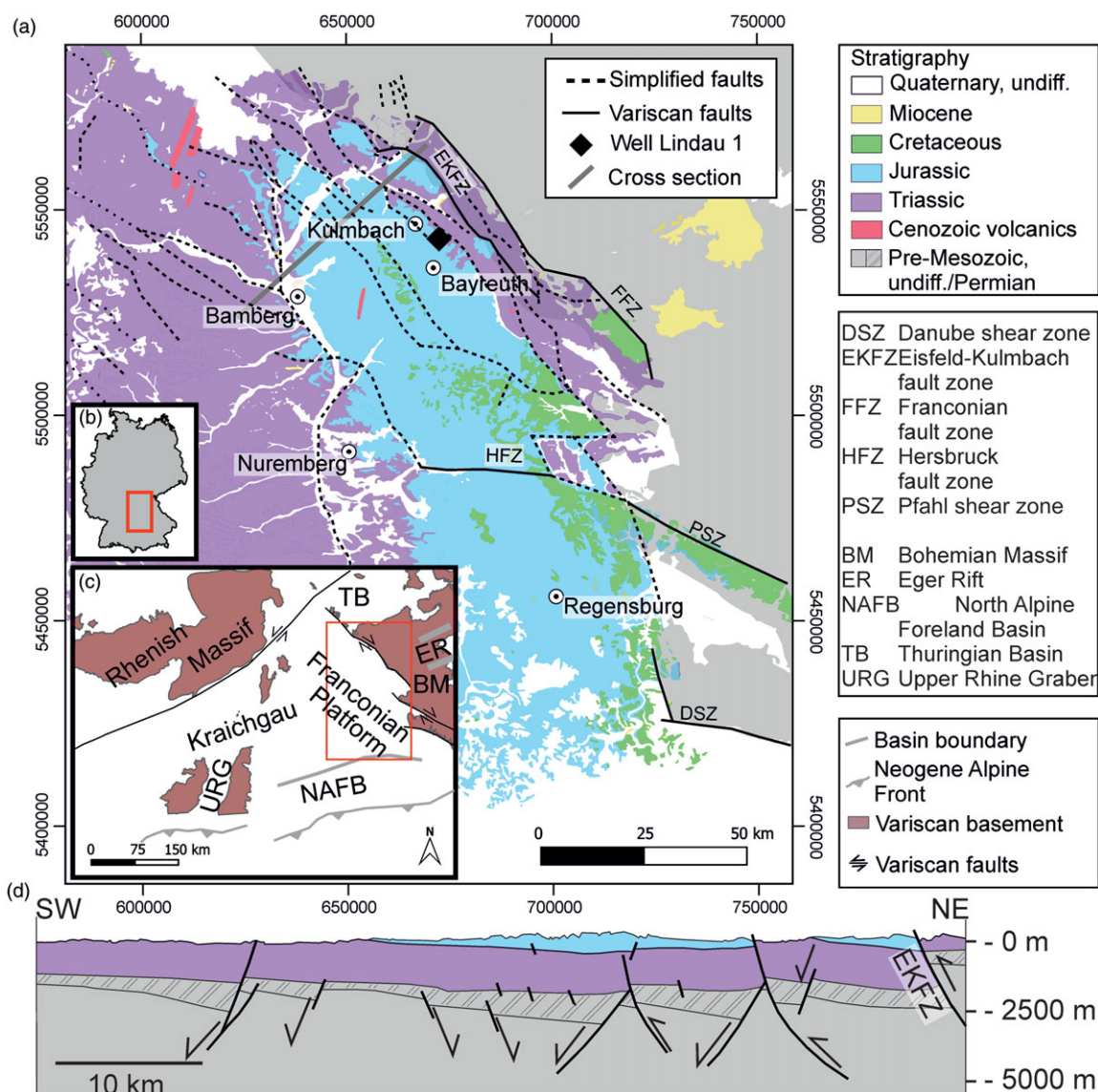


Fig. 1. (a) Simplified geological map of the study area (Digitale Geologische Karte von Bayern 1:25 000, 2020; available via https://www.lfu.bayern.de/geologie/geo_karten_schriften/dgk25_uab/index.htm) showing the location of Lindau 1 drill site. (b) Position of the study area (red rectangle) in the frame of the German borders. (c) Location of the study area (red rectangle), including the Franconian Platform in a Central European context (simplified after Dèzes *et al.* 2004), showing exposures of Variscan basement, major Variscan strike-slip faults, the Neogene Deformation Front, the North Alpine Foreland Basin and other important Cenozoic basins. (d) NE–SW-directed cross-section through the northern part of the study area, simplified after Fazlikhani *et al.* (2022).

Reicherter *et al.* (2008) and Heidbach *et al.* (2016), who claim that the present-day stress field in our study area is dominated by N(N) W–S(S)E-directed compression.

3. Methods

In order to reconstruct palaeostress fields, we combine two methods, fault-slip analysis (Angelier, 1984) and stylolite stress inversion (Koehn *et al.* 2012; Beaudoin *et al.* 2016). In addition to faults and stylolites (e.g. Figs 2a and 3b), we use related structures such as folds (e.g. Fig. 2c), joints and veins to derive relative age relationships from field studies. We apply the term *fracture* for brittle deformation structures (e.g. joints) without fault planes on the metre scale in outcrops, whereas the term *fault* (F) is used for fault planes on metre scale as well as in outcrop scale (50 to 1000 m). We apply the term *fault zone* (FZ) for fault planes on map scale (1 to

100 km). A fault zone may include a set of sub-parallel faults with similar kinematics. We assume that large single faults that would fit this definition form an exception in our study area.

Coordinates, lithologies and stratigraphic positions of all field measurement locations are summarized in Table 1. We pooled the direction measurements into key outcrop groups according to their geographical location, their relation to large-scale faults and the sedimentary facies. Most of the outcrops are located in carbonate rocks. All locations in outcrop group 1 (Franconia North) are stratigraphically positioned in the Middle Triassic (Muschelkalk). Groups 2 and 3 (Kulmbach North and South; Figs 3a and 2c, respectively) are distinguished, based on a kink in the strike direction of the Eisfeld–Kulmbach FZ from NW–SE in its southern part towards WNW–ESE in the northern part. Groups 4 and 5 (Central Franconia and Reef Facies; Fig 2b and d, respectively) are Upper Jurassic (Malm) carbonate rocks located within the Franconian

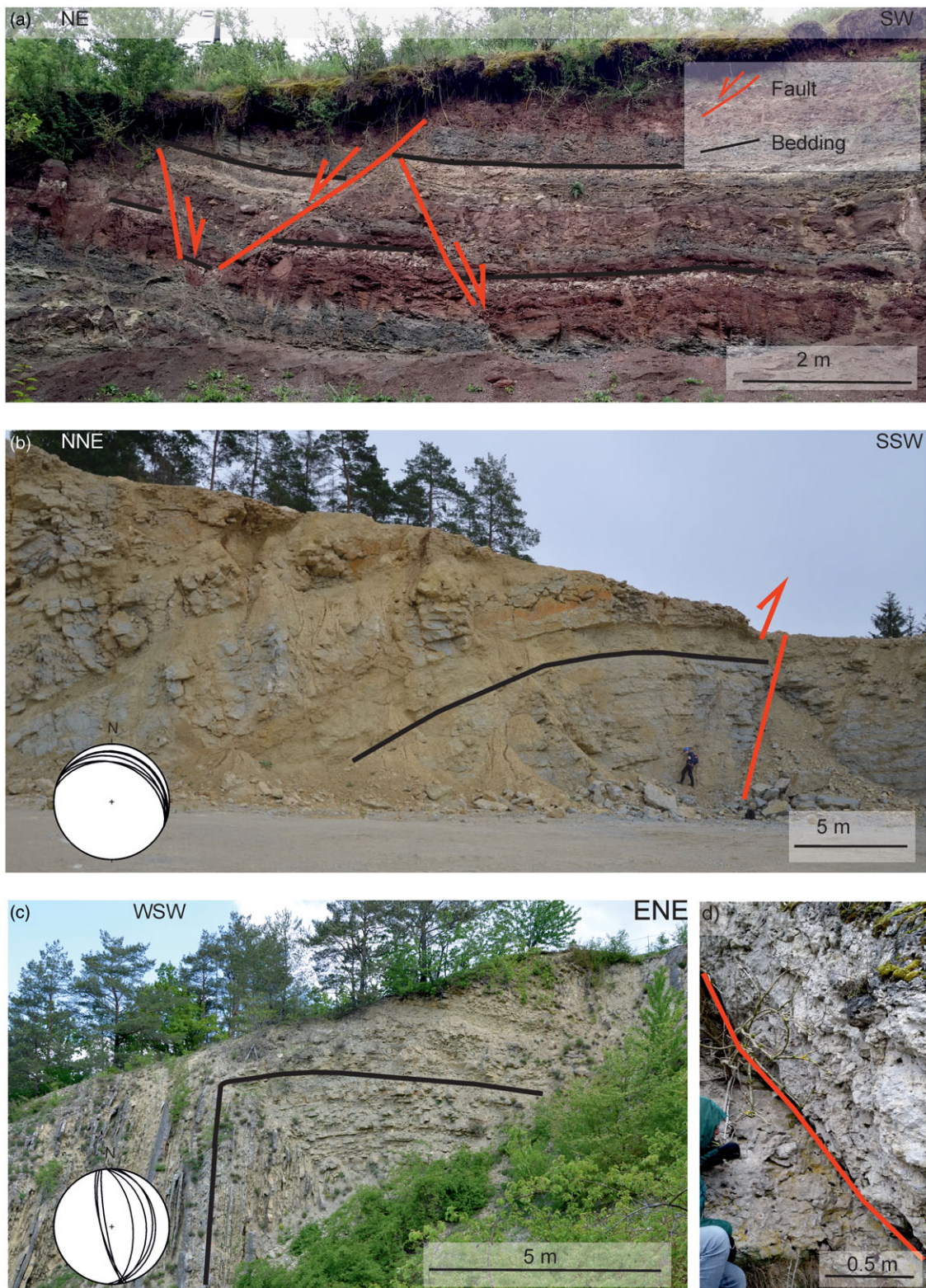


Fig. 2. (a) NE-striking wall of Upper Triassic Keuper sandstone in outcrop 9 (locality Kleinbardorf) showing NE- and SW-dipping normal faults. (b) Fold in the active quarry of outcrop 4b (locality Serkendorf), in Upper Jurassic (Malm) limestones, resulting from SSW-NNE compression. The inset shows the orientation of bedding planes in a stereographic projection (lower hemisphere). (c) Photo from outcrop 3b (locality Herlas), showing a WSW-vergent fold in Middle Triassic (Muschelkalk) limestones. The inset shows the orientation of bedding planes in a stereographic projection (lower hemisphere). (d) Field picture from outcrop 5b (locality Königsfeld). The visible feature is interpreted as a fault plane with unknown sense of slip.

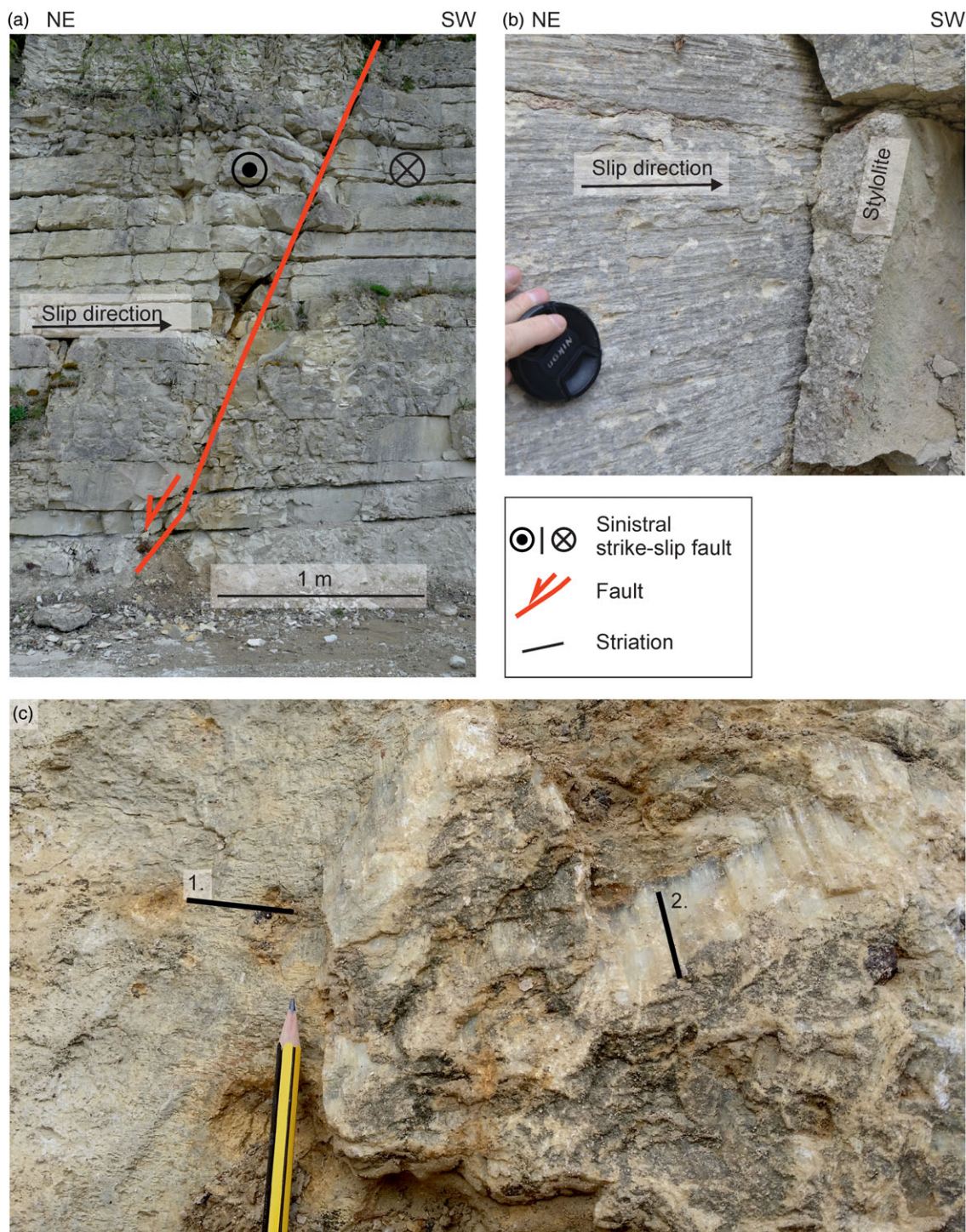


Fig. 3. (a) Outcrop photo from group 2 (locality Kirchleus), exposing Jurassic limestones showing a NE-striking dextral fault plane, cross-cut by (i) normal and (ii) sinistral strike-slip faults. (b) Photo in close proximity to (a), showing the dextral strike-slip fault offsetting a tectonic stylolite with NE–SW-directed teeth. (c) Outcrop photo from group 10 (locality Hartmannshof), showing striations two directions. The small numbers indicate the relative chronology.

Platform, with group 4 consisting of layered limestone and group 5 consisting of massive reef dolomite. Group 7 (Nuremberg) is distinguished from the neighbouring locations of groups 6 and 10 (Erlangen and Hersbruck, respectively) due to its location south of the W–E-striking Hersbruck FZ and because it has a high amount of stylolites with a low amount of fault planes (see Section 4a below and Fig. 4). Group 8 is defined by the location of the outcrops in the

south of the study area with a large extension in E–W direction. Group 9 includes outcrops of Upper Triassic (Keuper) sedimentary rocks (Fig. 2a). Tectonic stylolites are rough surfaces formed by pressure solution (Park & Schot, 1968). They are associated with layer-parallel shortening tangential to the bedding. Stylolite teeth grow parallel to the largest principal stress σ_1 (Nitecki, 1962; Koehn *et al.* 2007). Thus, a stylolite plane with orthogonal teeth is

Table 1. Outcrop information

Group	Location	Longitude	Latitude	Lithology	Stratigraphy		
1	Franconia North	a	Fornbachtal	11.002399	50.32707	Limestone	Middle Triassic
		b	Fechheimer Berg	11.076566	50.27913	Limestone	Middle Triassic
2	Kulmbach North	Kirchleus	11.37065	50.18112	Limestone	Upper Jurassic + Middle Triassic	
3	Kulmbach South	a	Unterdornlach	11.404753	50.15024	Limestone	Middle Triassic
		b	Herlas	11.471117	50.08044	Limestone	Upper Jurassic
4	Central Franconia	a	Azendorf	11.312727	50.02973	Limestone	Upper Jurassic
		b	Serkendorf	11.122142	50.07578	Limestone	Upper Jurassic
		c	Wattendorf	11.1168821	50.04119	Limestone	Upper Jurassic
5	Reef Facies	a	Paradiesttal	11.185627	49.99052	Dolomite	Upper Jurassic
		b	Königsfeld	11.176197	49.94938	Dolomite	Upper Jurassic
		c	Görau	11.309736	50.05761	Dolomite	Upper Jurassic
		d	Würgau	11.101322	49.97813	Dolomite	Upper Jurassic
6	Erlangen	a	Ebermannstadt	11.18571	49.79209	Limestone	Upper Jurassic
		b	Leutenbach	11.18642	49.70408	Limestone	Middle–Upper Jurassic
		c	Forchheim	11.006698	49.72556	Limestone	Lower Jurassic
		d	Ebermannstadt 2	11.167379	49.78452	Limestone	Upper Jurassic
7	Nuremberg	a	Schupf	11.488153	49.44942	Limestone	Upper Jurassic
		b	Oberrieden	11.404297	49.40777	Limestone	Upper Jurassic
		c	Happurg	11.479136	49.4964	Marlstone	Middle Jurassic
		d	Weißbrunn	11.372413	49.42492	Limestone	Upper Jurassic
8	Franconia South	a	Neuburg a.d. Donau	11.12488	48.92365	Limestone	Upper Jurassic
		b	Leibrecht	11.5384615	49.02033	Limestone	Upper Jurassic
		c	Dietfurt	11.6143724	49.03222	Limestone	Upper Jurassic
		d	Deurling	11.9042248	49.03823	Limestone	Upper Jurassic
		e	Blumenberg	11.148827	48.90167	Limestone	Upper Jurassic
		f	Saal a.d. Donau	11.941808	48.88757	Limestone	Upper Jurassic
9	Heldburg	Kleinbardorf	10.424538	50.28057	Marlstone	Upper Triassic	
10	Hersbruck	Hartmannshof	11.554999	49.50204	Limestone	Middle Jurassic	

perpendicular to the σ_1 direction. However, there is a continuous transition from stylolites associated with layer-parallel shortening through stylolites with tilted planes and oblique teeth and slickolites that develop on fault planes where teeth still preserve the direction of the σ_1 (Nitecki, 1962; Koehn *et al.* 2007, 2012; Toussaint *et al.* 2018). The intermediate and smallest principal stresses σ_2 and σ_3 lay in the stylolite plane. Field observations, however, do not allow determination of their exact orientations (Schmittbuhl *et al.* 2004; Ebner *et al.* 2010).

Here, we recorded tectonic stylolites as planar features with dip angle and dip direction together with the azimuth of the stylolite teeth as linear features.

Measured faults are categorized into three groups according to the quality of the measurement and the reliability of their sense of movement indicators (sides of steep teeth) (Sippel *et al.* 2009; Sperner & Zweigel, 2010). We measured a total of 546 faults and 432 tectonic stylolites at 28 locations (Table 1; Figs 5, 6); all data are available online via <https://doi.pangaea.de/10.1594/PANGAEA.929490> (Köhler *et al.* 2021).

The stress history based on fault-slip inversion (PBT axes method) was reconstructed using the software *Tectonics FP* (Reiter & Acs, 2020). The PBT method is based on the assumption that fault planes develop at an angle of 30° to σ_1 (Anderson, 1972). This is in agreement with the observation that conjugate fault planes form angles of *c.* 60° . For each fault-slip datum the respective P- (compressional axis, σ_1), B- (neutral axis, σ_2) and T- (tensional axis, σ_3) were constructed graphically (Turner, 1953; Ortner *et al.* 2002). Following Sippel *et al.* (2009), we subdivided the calculated data into distinct homogeneous clusters of PBT axes orientations. Following Wallbrecher (1986), *Tectonics FP* calculates the mean vectors and concentration parameter R% (Ortner *et al.* 2002). We excluded faults which do not fall into a cluster with at least ten data points and with a minimum R% value of 90%. We constructed clusters for (i) the entire working area, defining superordinate stress fields, and (ii) the aforementioned outcrop groups to analyse local variations in stress orientation, and compared these to mapped faults. To perform the palaeostress inversion at local resolution, the locations were split into ten groups as explained before (Table 1).

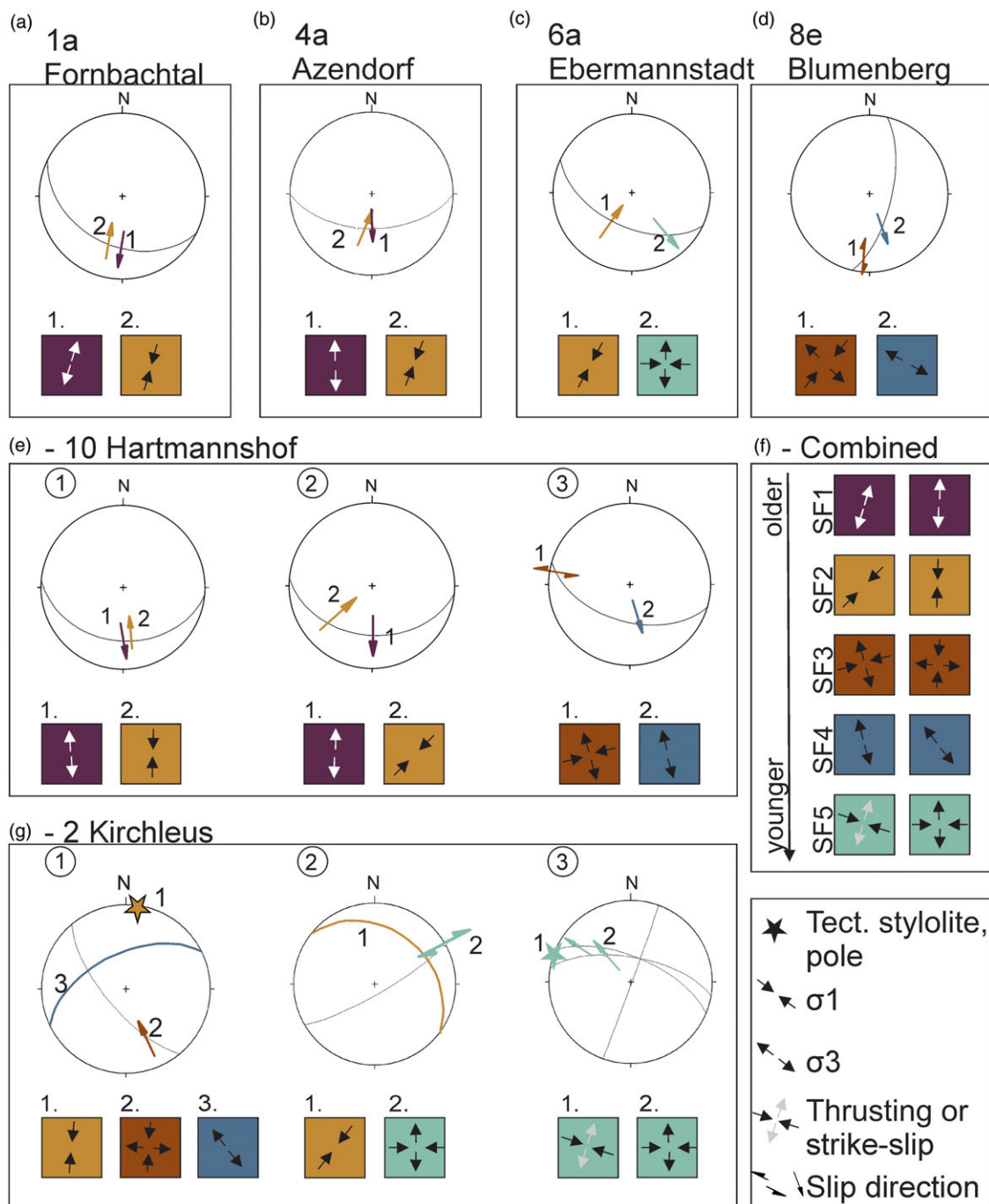


Fig. 4. Single measurements of fault planes and fault lineation (if applicable) and their relative chronology (based on cross-cuttings and multiple striations), plotted as stereographic projection, lower hemisphere. Kinematic directions of the single measurements can differ from the overall stress fields. Boxes beneath projections and on the right show the schematic direction of the highest (inward arrows) and lowest (outward arrows) horizontal stresses (map view, against north) in their relative chronological order. Colours refer to the stress field. See Table 1 for further details on outcrop groups.

A stress field is defined by spatial uniformity or variability of a certain aspect of the stress tensor that persisted over a certain time in the geological past. Here, we use the following terms to describe a stress field: The magnitude of the vertical stress (σ_v) is the integral of the weight of the overburden. Only at the Earth's surface is σ_v a principal stress axis of the stress tensor whereas σ_v can deviate from a principal stress orientation at greater depths. When σ_v is a principal stress axis, the maximum and minimum horizontal stresses (σ_{Hmax} and σ_{Hmin}) are the other two principal stresses. Otherwise, σ_{Hmax} and σ_{Hmin} are the projections of the principal

stresses into the horizontal plane. The stress regime is considered as the expression of the relative magnitudes of the principal stresses. Tectonic regimes are termed 'normal faulting' when $\sigma_v > \sigma_{Hmax} > \sigma_{Hmin}$; 'thrust faulting' when $\sigma_{Hmax} > \sigma_{Hmin} > \sigma_v$; and 'strike-slip' when $\sigma_{Hmax} > \sigma_v > \sigma_{Hmin}$ (cf. Zoback & Zoback, 1989). It is worth noting that only when faults are optimally oriented in the stress field does the stress regime coincide with the tectonic regime.

After the clustering into stress fields, we calculated shifts between (i) the superordinate stress fields and (ii) the local stress

	Stress fields in chronological order					Styolite density
	SF1	SF2	SF3	SF4	SF5	
<div style="display: flex; align-items: center;"> <div style="width: 15px; height: 15px; border: 1px solid black; margin-right: 5px;"></div> Compressive <div style="width: 15px; height: 15px; background-color: gray; margin-right: 5px;"></div> Tensile </div>						
Super-ordinate stress field	σ_3 in N-S direction	σ_1 in N-S to NE-SW direction	Strike-slip with σ_1 in NE-SW direction	σ_3 in N-S to NW-SE direction	Strike-slip with σ_1 in (W)NW-(E)SE	
1. Franconian North	N = 2	N = 2	N = 4		N = 3	N = 5
2. Kulmbach North	N = 7	N = 10	N = 17		N = 8	N = 152
3. Kulmbach South					N = 8	N = 14
4. Central Franconia		N = 9	N = 14		N = 9	N = 113
5. Reef Facies	N = 3	N = 7			N = 3	N = 5
6. Erlangen	N = 3	N = 4		N = 6	N = 5	N = 25
7. Nuremberg						N = 60
8. Franconian South	N = 4		N = 3	N = 5	N = 5	N = 45
9. Heldburg	N = 2			N = 7	N = 7	
10. Hersbruck	N = 12	N = 7	N = 13	N = 4	N = 3	N = 13

Fig. 5. Beachball plots and stereographic projections (lower hemisphere) of all analysed faults and inferred stress fields 1–5. The rightmost column shows density plots of the measured tectonic stylolites. See Table 1 for further details on outcrop groups, individual locations and their coordinates, lithologies and stratigraphy.

fields. For simplification we assume that two principal stresses of the stress tensor are oriented in a horizontal plane according to Anderson’s theory (Anderson, 1972). Variation is then calculated as the azimuthal difference in degree between (i) and (ii), resulting in a clockwise or anticlockwise shift.

The use of fault-slip data for stress inversion is applicable, if the following assumptions outlined by Anderson (1972) and Sperner

and Zweigel (2010) apply: (1) measurements of the slip data in small outcrops are representative of the far-field stress; (2) rotation of fault-bounded blocks (100 m to km scale) has not distorted the stress marker significantly; (3) the material is homogeneous enough to allow retrieval of the incremental strain that can then be transferred to the stress through stress inversion; (4) different stress fields can be separated by the data; and (5) the orientation

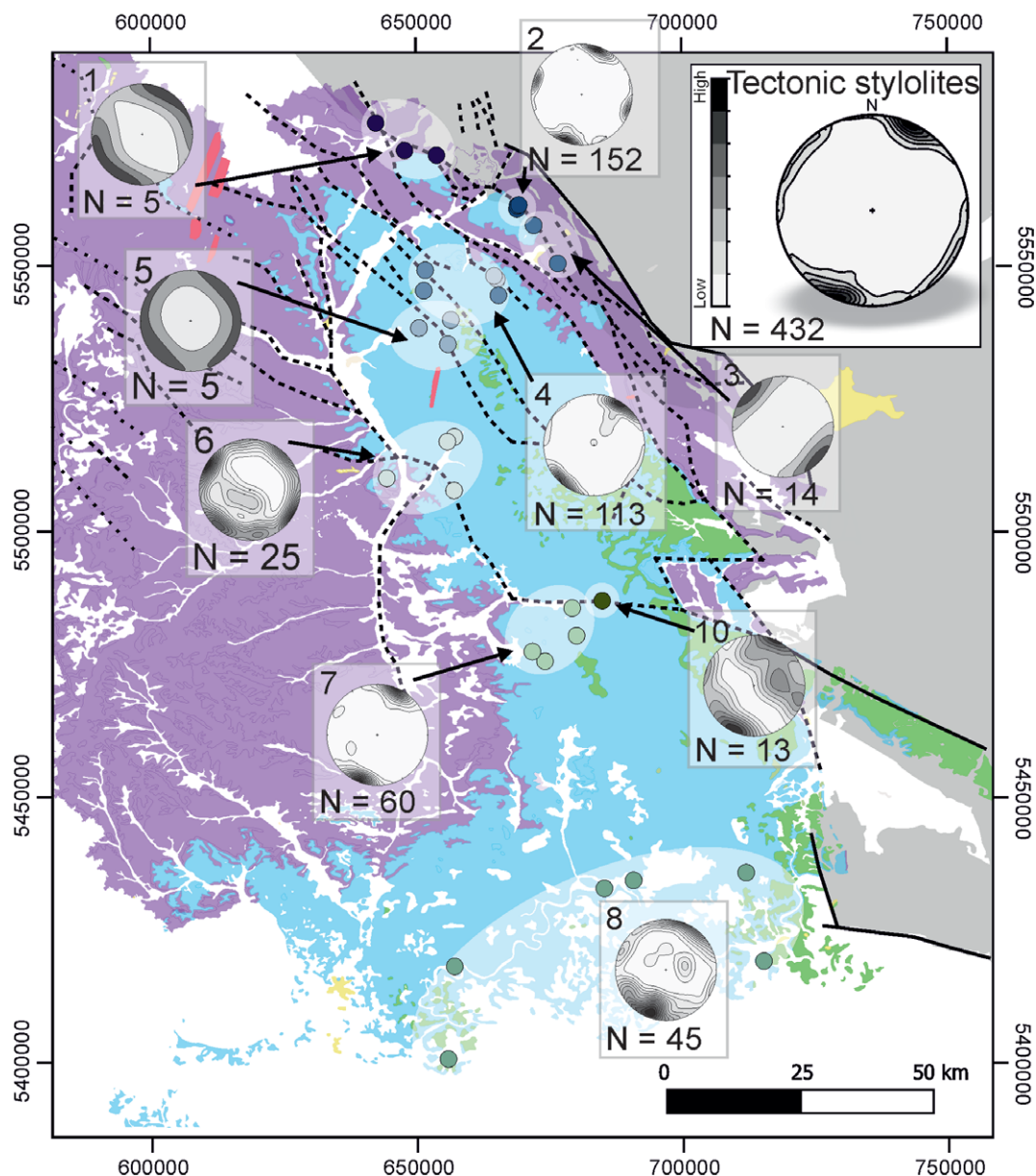


Fig. 6. Geological map showing the distribution of tectonic stylolites as density plots (stereographic projection, lower hemisphere) for the individual outcrop groups and for the entire study area (top right). See Figure 1 for key to colours. See Table 1 for further details on outcrop groups.

of σ_1 relative to the fault's dip is 30° at close-to-surface conditions, which is the case in most situations in the field where we can observe conjugate fault sets.

To increase validation and representability (assumption 1), we use a combination of two independent methods, i.e. fault-slip and tectonic stylolites. Using fault-slip inversion alone entails the risk of measuring artefacts of pre-existing fault zones. Those can produce perturbation of the applied stresses and therefore result in a heterogeneous stress pattern in the overall study area (Lacombe, 2012). We will discuss the validation of assumption 2, the negligibility of block rotation, in Section 5.c below. The Upper Jurassic carbonate rocks essentially comprise two lithofacies: (i) the dominant so-called 'normal facies', composed of well-bedded limestones and marls and (ii) the 'reef facies', build-ups formed by sponges and microbial crusts (algal-sponge reefs) and locally also by corals (Munk, 1980). The dominant 'normal facies' rocks are

relatively homogeneous in terms of their rheology. We assume that inhomogeneities associated with the visible layering do not have a strong effect at the outcrop or map scale especially where two principal stresses lay in the bedding plane. Thus, assumption 3 is valid, too. The dolomites of the 'reef facies', however, provide an exception (outcrop group 5, Reef Facies) as these are massive and strongly karstified. Compared to the other groups, fault-slip indicators are poorly preserved in outcrops of this group and therefore the number of measurements is low. Assumption 4, the separation of multiple stress fields, is valid for most of the data that fall clearly into distinct stress fields that can be separated. Data that cannot be statistically clustered are neglected in this study. Assumption 5 is valid because locally slickolites record directly the orientation of σ_1 relative to fault planes, the angle between the slickolite and the fault plane is 30° on average and conjugate fault planes form an angle of 60° . We used only faults with

preserved striation and slip direction for our analysis. The risk of missing minor structures or subjective interpretation of slip direction (Sperner & Zweigel, 2010) is minimized by the contributions of four persons to the final dataset (Köhler *et al.* 2021). All contributors are aware of the importance of distinguishing between slickenfibres, slickolites, stylolites and joints (Lisle, 2013). No outcrop was analysed by one single person.

4. Results

4.a. Stress fields and their relative age relationships

We identified five different stress field generations, causing brittle deformation, folding and the development of tectonic stylolites in the study area. The relative age relationships of these stress fields were determined through local observations of cross-cutting relationships of the respective structures and multiple striations (Figs 3, 4), yielding the following chronology (from old to young) of successive stress fields (SF):

1. Normal fault regime under N(NE)–S(SW) horizontal extension
2. Thrusting regime under N(E)–S(W) horizontal compression (cogenetic with the formation of a first set of tectonic stylolites)
3. Strike-slip regime under N(N)E–S(S)W horizontal compression and (W)NW–(E)SE-directed horizontal extension
4. Normal fault regime under N(N)W–S(S)E horizontal extension
5. Strike-slip regime under (N)W–(S)E horizontal compression and N(E)–S(W) horizontal extension (cogenetic with the youngest set of tectonic stylolites)

We correlate these SFs to the overall SFs (Section 4.c below). However, the observations yield very local information, and thus the orientation of the SFs can differ from the regional observations. Normal and reverse sense striations were preserved on the same W–E- to NW–SE-striking fault planes (Fig. 4a–b, e1, e2), resulting from N(NE)–S(SW) normal faulting regime (SF1) followed by NE–SW-thrusting regime (SF2), respectively. Due to the stratigraphic age of the analysed outcrops (Table 1), the maximum age of SF1 is Late Jurassic (Malm). SF2 is associated with tectonic stylolites indicating NE–SW compression that are rotated by SW-vergent folds (Fig. 2c). We observed cross-cutting relationships between those stylolites and dextral NW–SE-striking faults (Figs 3b, 4g1) that are indicative for a younger strike-slip regime with a roughly N-trending σ_1 and E-trending σ_3 (SF3). In addition, SF3 strike-slip faults are cutting straight through SF2-related folds. At three locations we observed overprinting of SF3 by N(N)W–S(S)E normal faults associated with SF4. While both SF2 stylolite and SF3 dextral faults are cross-cut by NW-dipping normal faults (SF4) in group 2 (outcrop 2, Kirchleus in Figs 3a, 4g1), SF3 strike-slip faults are reactivated as SF4 normal faults in outcrops 10 and 8b (Figs 3c, 4d, e3).

In addition, SF2 thrusts and reverse faults are overprinted by oblique, NW-striking normal faulting (Fig. 3a) and cross-cut by dextral NE-trending faults (Figs 3b, 4g2), both resulting from a strike-slip regime with an E-trending, horizontal compression (SF3). The younger set of tectonic stylolites show a (W)NW–(E)SE horizontal compression that is related to SF5. These stylolites are cross-cut by dextral WNW-trending fault planes (Fig. 4g3). While these youngest faults are associated with a strike-slip regime under E–W horizontal compression, the younger stylolites could be related to either thrusting (i.e. vertical σ_3) or strike-slip (i.e. horizontal σ_3 ; Ebner *et al.* 2010). The stress field related to the youngest set of stylolites resembles the one associated with the

youngest set of strike-slip faults (SF5). However, there is a lack of clear evidence of age relationships between SF4 and SF5. Unambiguous cross-cutting relationship between structures correlating with SF4 and SF5 have not been observed.

4.b. Stylolites and folds

Tectonic stylolites are well developed in Upper Jurassic (Malm) limestones, while their development in dolomites or in Middle Triassic (Muschelkalk) limestones is limited (groups 5 and 1, respectively). In sandstone-dominated lithologies we observed no stylolites at all (group 9). The preferred orientations of the measured stylolites are shown as density plots in Figures 5, 6. As stylolite teeth grow parallel to σ_1 , a maximum in the density plot corresponds to the direction of σ_1 . In the Franconian North outcrop group 1, rare tectonic stylolites suggest a bimodal distribution of their orientation, i.e. the coexistence of NNE–SSW- and W–E-directed teeth (Figs 5, 6). Orientation of stylolite teeth in the Kulmbach area varies from bimodal, NNE–SSW- and NW–SE-directed teeth (Kulmbach North, group 2) to unimodal NW–SE-directed teeth (Kulmbach South, group 3) (Figs 5, 6). In the hanging wall of the NE-dipping Eisfeld–Kulmbach FZ (Figs 6 and (further below) 8, outcrop 3b) oblique tectonic stylolites are observed in Muschelkalk limestones of an overturned fold limb (Fig. 2c). Throughout the entire Kulmbach area, fold axes trend NNW–SSE ((further below) Fig. 8). In Central Franconia (group 4) tectonic stylolites show a bimodal distribution in orientation, with the most dominant maximum indicating horizontal compression in the NE–SW direction, and a minor maximum in a NW–SE direction (Fig. 5). Around Erlangen (group 6), tectonic stylolites record NW–SE- and NE–SW-directed horizontal compression (Figs 5, 6, group 6). In Nuremberg (group 7), tectonic stylolites record only a single maximum revealing NNE–SSW horizontal compression (Figs 5, 6). In Franconia South (group 8) the majority of stylolite teeth trend NE–SW and a smaller population records the WNW–ESE horizontal compression (Figs 5, 6). In Hersbruck (group 10), stylolite teeth predominantly trend NNE–SSW, with a minority trending NW–SE.

4.c. Overall stress field and local deviations

For each stress field and each outcrop group we created beachball plots, with the largest (σ_1) and the lowest (σ_3) principal stress axis in the centre of the white and grey quadrants respectively. The intersection of the quadrants gives the orientation of σ_2 . To visualize local variations in the respective stress fields we compiled the beachball plots on geological maps for each stress field (Figs 7–11). The local shift of the stress directions with respect to the regional stress orientation is collected in Tables 2–6.

4.c.1. Normal fault regime under N(NE)–S(SW) horizontal extension (SF1)

The oldest stress field (SF1) is constrained from 23 normal faults (e.g. Fig. 2a) that have a NNE–SSW-directed σ_{hmin} with an R-value of 90–92 % in the fault-slip inversion. σ_1 is sub-vertical with an orientation of 215/85 (i.e. $\sigma_1 = \sigma_v$) and σ_3 is sub-horizontal-trending (N)NE–(S)SW (035/05, $\sigma_3 = \sigma_{\text{hmin}}$). Along the Hersbruck FZ the regional principal stress direction deviates clockwise by 28° from the superordinate stress field towards a more N–S-trending σ_{hmin} (Table 2) whereas beachball plots from the other areas illustrate NE–SW-trending σ_{hmin} (Fig. 7).

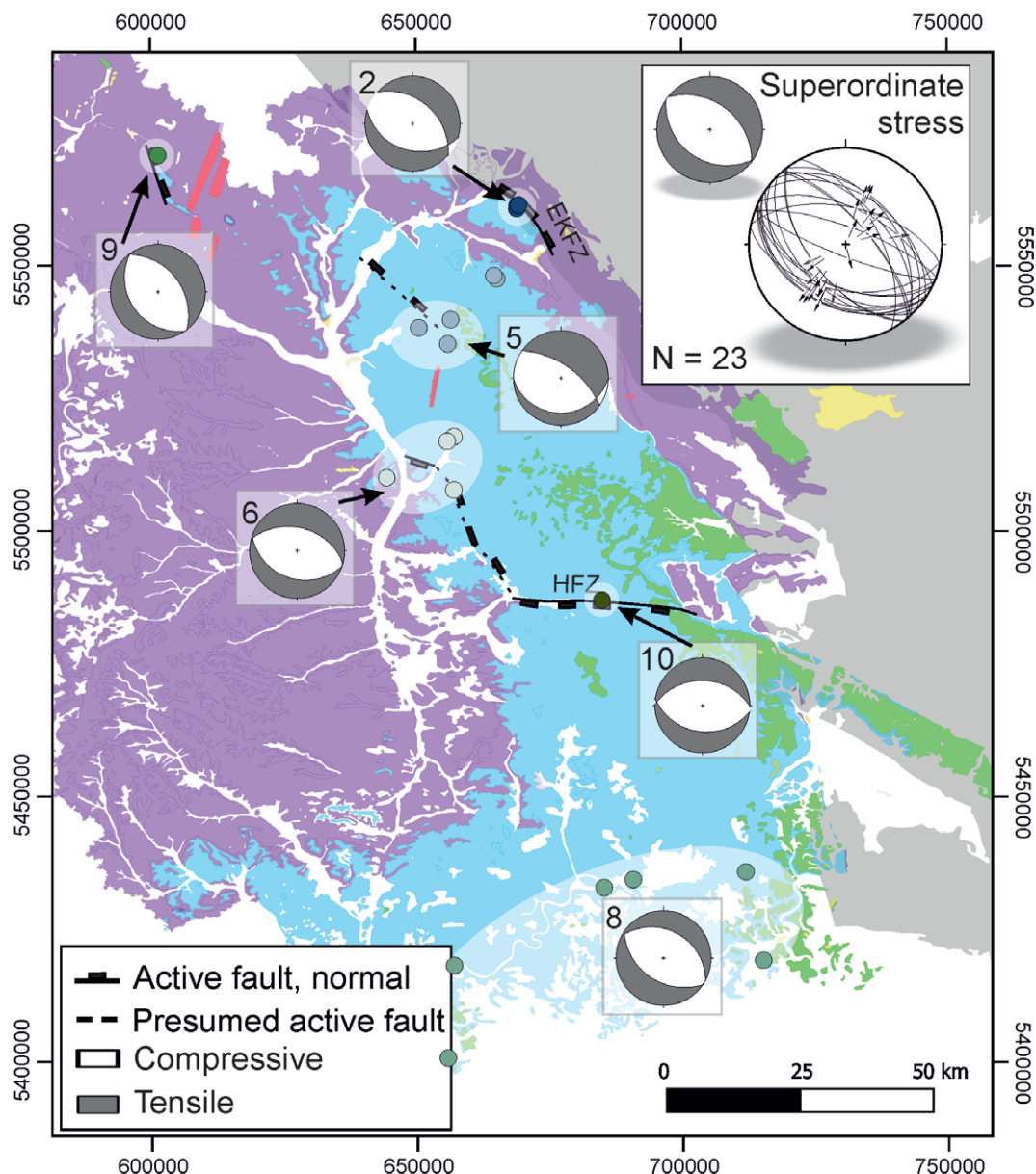


Fig. 7. Beachball plots illustrating regional variability of SF1 and prevailing N–S to NE–SW extension. Straight black lines of the map show active, dashed lines probably active faults during SF1. Top right: beachball plot and stereographic projection (lower hemisphere) of SF1-related faults with slip sense. Abbreviations: EKFZ – Eisfeld–Kulmbach fault zone; HFZ – Hersbruck fault zone. See Figure 1 for key to colours and Table 1 for further details on outcrop groups.

4.c.2. Thrusting regime under NNE–SSW- to NE–SW- directed horizontal compression (SF2)

The second stress field (SF2) is compressive with a NNE–SSW σ_{Hmax} trend as obtained from 20 WNW–ESE- to NW–SE-striking thrust faults. Striations show that fault planes of SF1 were reactivated as reverse faults during SF2 (Fig. 4b, e1–2), e.g. the Hersbruck FZ (Fig. 8). Our stress inversion yields a horizontal orientation of 202/01 for σ_1 (i.e. $\sigma_1 = \sigma_{Hmax}$) with an R-value of 97 %, and a sub-vertical orientation of 299/85 for σ_3 ($= \sigma_v$) with an R-value of 96 %. We also observed several SW-vergent folds in Muschelkalk units with an overturned, steep limb in the hanging wall of the Eisfeld–Kulmbach FZ (Fig. 2c). These folds rotated some tectonic stylolites, indicating that layer-parallel shortening predated SF2

thrusting and folding. Further west in the study area, several open folds developed in Central Franconia (Fig. 2b). The density distribution of their tectonic stylolite teeth (Fig. 6) shows a maximum at 205°, i.e. parallel to the orientation of σ_{Hmax} derived from fault-slip analysis (Fig. 8). Locally the σ_{Hmax} direction may vary slightly, especially proximal to the Eisfeld–Kulmbach FZ. At Kulmbach South (group 3) for instance, NE–SW-directed tectonic stylolites and NW–SE-striking thrusts are not observed whereas at Kulmbach North (group 2), NW–SE-striking thrusts and NE–SW-trending tectonic stylolite teeth are common (Figs 4–6). SF2 is the most consistent stress field in our study area in terms of its orientation, with a minor scatter of $\pm 4^\circ$ around the mean orientation of σ_{Hmax} (Table 3).

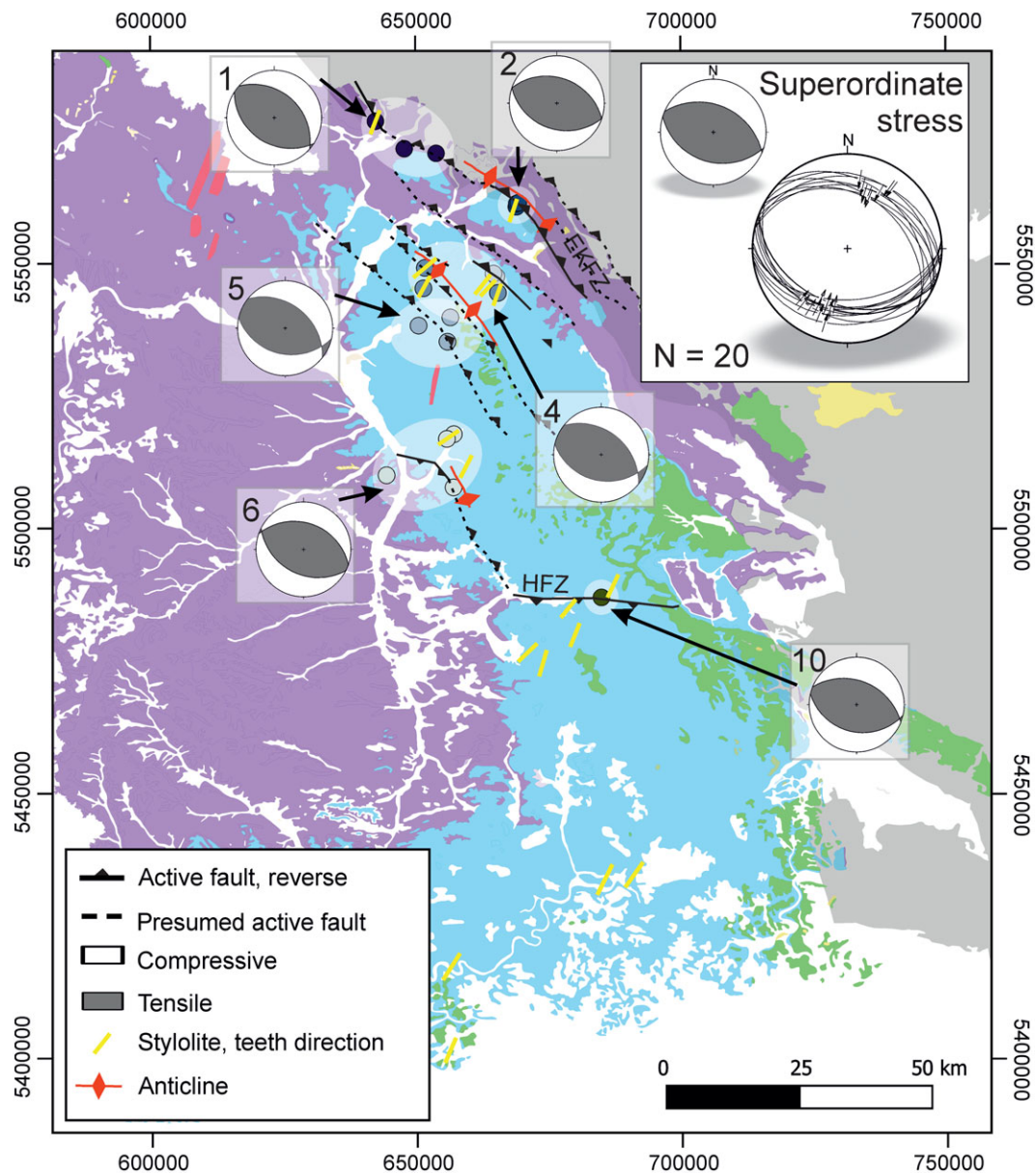


Fig. 8. Beachball plots illustrating regional variability of SF2 and prevailing NE-SW compression. Straight black lines show active, dashed lines probably active faults during SF2. Top right: beachball plot and stereographic projection (lower hemisphere) of SF2-related faults with slip sense. Teeth direction of tectonic stylolites is shown as yellow dashes, anticlines as red lines. Abbreviations: EKfZ – Eisfeld-Kulmbach fault zone; HFZ – Hersbruck fault zone. See Figure 1 for key to colours and Table 1 for further details on outcrop groups.

4.c.3. Strike-slip regime under NE-SW horizontal compression and NW-SE horizontal extension (SF3)

SF3 is inferred from 25 strike-slip faults, of which 17 strike NNE-SSW to NE-SW with dextral slip sense and 8 strike E-W with a sinistral sense of slip. With an R-value of 92 %, σ_1 is oriented horizontally with an azimuth of 46° ($\sigma_1 = \sigma_{Hmax}$). σ_3 is horizontal with an orientation of 315/05 and an R-value of 94 % ($\sigma_3 = \sigma_{Hmin}$). Locally, reactivated faults show striations indicating successive normal faulting, reverse faulting and strike-slip. The strike-slip faults associated with this stress field are the most abundant faults (Fig. 3b) in the study area and often extend across whole quarries (100 m to km scale). Some mineralized extensional veins oriented 115/85 and 100/85 were

reactivated as dextral strike-slip faults by this stress field. There are also WNW-ESE-striking fault planes with sub-horizontal striations, implying a NNE-SSW-directed horizontal σ_1 and an oblique, non-vertical σ_2 and σ_3 , e.g. in group 3 (Fig. 12b, Section 5c below).

The orientation of SF3-related faults and the respective σ_{Hmax} and σ_{Hmin} orientations vary across the region. For example, at location 10 the strike of sinistral faults is sub-parallel to the E-W-striking Hersbruck FZ (Fig. 9), whereas in outcrop 2 faults strike NE-SW (Figs 9, 12c). In Kulmbach North the horizontal principal stress axes σ_1 and σ_3 vary with 34° and 33° anticlockwise from the superordinate stress field recording NNE-SSW compression (i.e. σ_{Hmax}) and WNW-ESE extension (σ_{Hmin}). In contrast, in group

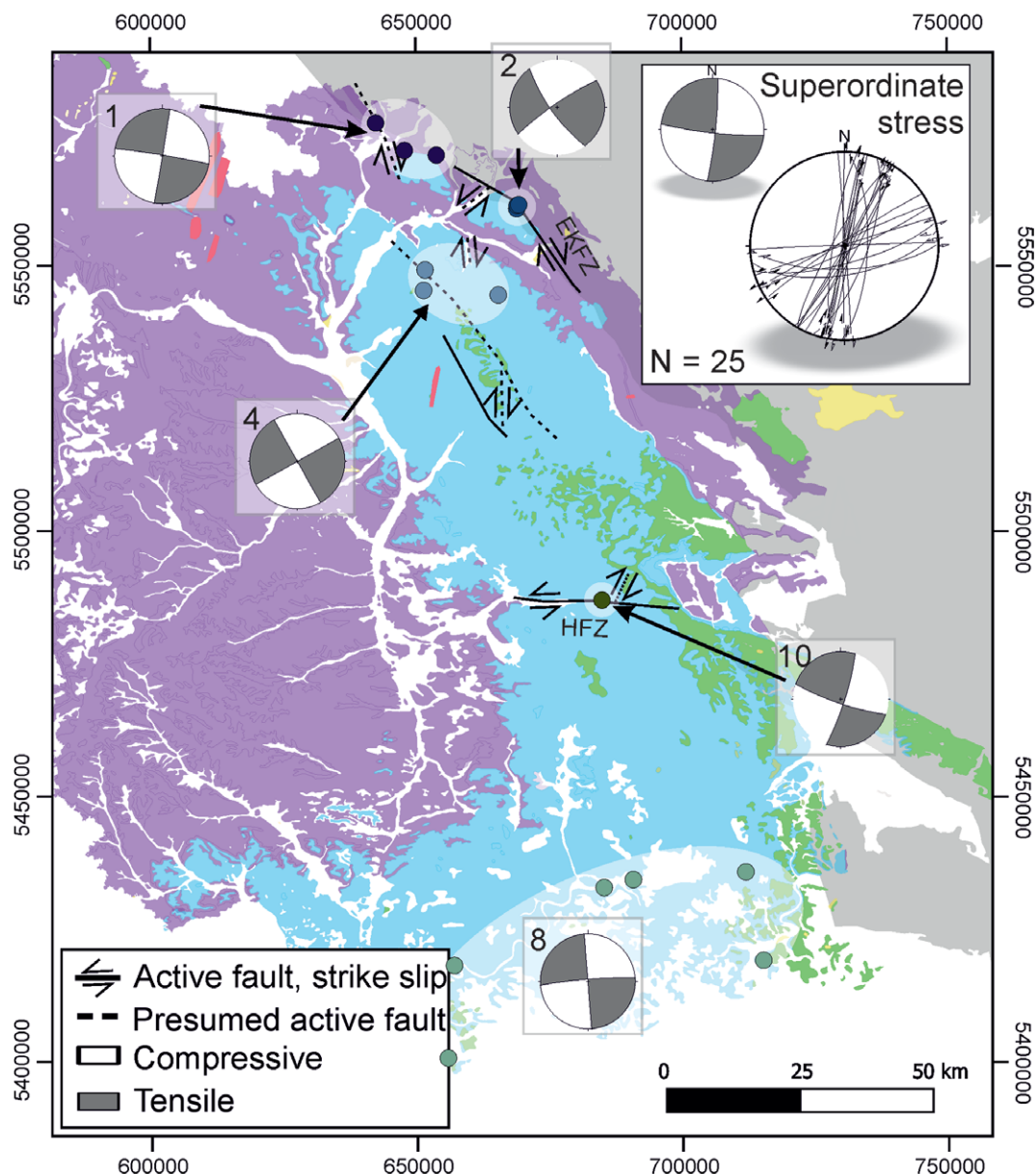


Fig. 9. Beachball plots illustrating regional variability of SF3 and prevailing NE–SW compression with NW–SE extension. Straight black lines show active, dashed lines probably active faults during SF3. Top right: beachball plot and stereographic projection (lower hemisphere) of SF3-related faults with slip sense. Abbreviations: EKFZ – Eisfeld–Kulmbach fault zone; HFZ – Hersbruck fault zone. See Figure 1 for key to colours and Table 1 for further details on outcrop groups.

10 the stress axes σ_{Hmax} and σ_{hmin} are shifted clockwise by 13° and 14° , indicating ENE–WSW-trending σ_{Hmax} and NNW–SSE σ_{hmin} (Table 4).

4.c.4. Normal fault regime under NW–SE-directed horizontal extension (SF4)

NW–SE-directed extension is identified from 14 predominantly SE-dipping normal faults. The associated conjugate set of NW-dipping faults occurs less frequently and is restricted to the Erlangen outcrop group (group 6; Fig. 5). Fault-slip inversion leads to a (sub-)vertical σ_1 orientation of 215/87 ($\sigma_1 = \sigma_v$), within an R-value of 90%. σ_3 is oriented horizontally, with 137/01 within an R-value of 90% ($\sigma_3 = \sigma_{hmin}$). Due to the poor preservation of this stress field over the entire working area, we were only able to calculate local stress fields for four outcrop groups (Fig. 10).

Therefore, the activity of fault zones at larger scales is only assumed. Relative to the overall mean direction, measured SF4 σ_{hmin} directions vary from 15° anticlockwise (ESE–WNW) in group 9, to 10° clockwise ((S)SE–(N)NW) in group 10 (Table 5).

4.c.5. Strike-slip regime under NW–SE horizontal compression and NE–SW horizontal extension (SF5)

Nine ENE–WSW-striking dextral strike-slip faults and 11 NNW–SSE-striking sinistral strike-slip faults are included in subset SF5. σ_1 (126/03, $\sigma_1 = \sigma_{Hmax}$) and σ_3 (216/00, $\sigma_3 = \sigma_{hmin}$) are horizontal with an R-value of 93% and 91%, respectively. This orientation of σ_1 is in agreement with the minor maximum of tectonic stylolites (Fig. 5). This configuration indicates a strike-slip regime with horizontal compression in a NW–SE direction of σ_{Hmax} and NE–SW trending σ_{hmin} . As derived from measured strike-slip and oblique

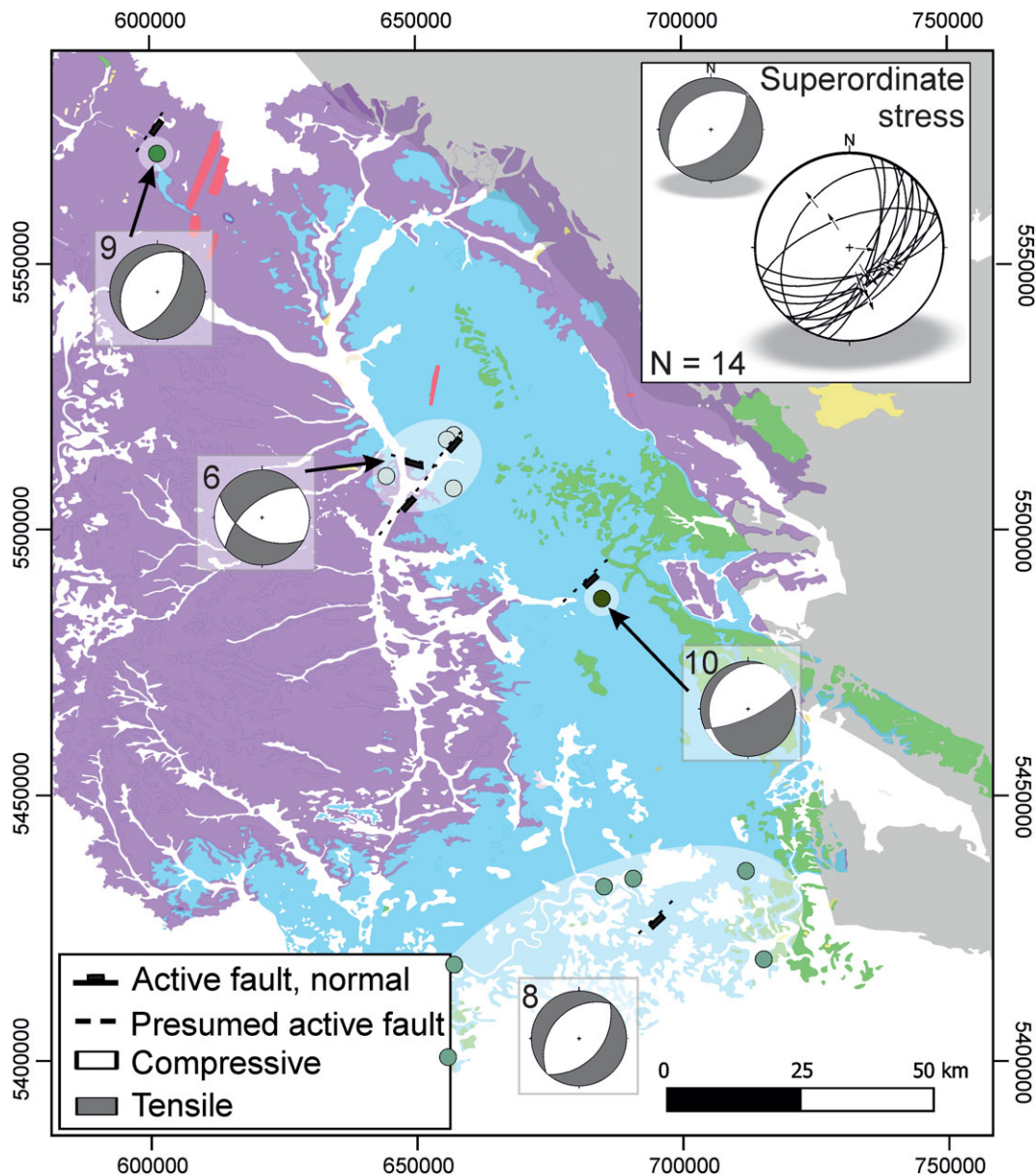


Fig. 10. Beachball plots illustrating regional variability of SF4 and prevailing NW–SE to N–S extension. Straight black lines show active, dashed lines probably active faults during SF4. Top right: beachball plot and stereographic projection (lower hemisphere) of SF4-related faults with slip sense. See Figure 1 for key to colours and Table 1 for further details on outcrop groups.

normal faults (Fig. 3a), SF5 is characterized by a high variability in fault orientations relative to the principal stress axes (Figs 5, 11). In addition, the direction of σ_{Hmax} varies considerably across the study area. For example, at Franconia North (group 1) and Kulmbach North (group 2), σ_{Hmax} deviates clockwise by 21° and 43° from its average orientation and σ_{Hmin} varies with 30° and 47° clockwise (Table 5). Both deviations show a strong local shift from the dominating (E)SE–(W)NW-trending σ_{Hmax} towards a more SSE–NNW-directed σ_{Hmax} . Directions of associated tectonic stylolites vary as well (Figs 5, 11), with stylolites in Kulmbach South (group 3) indicating horizontal compression in a NW–SE direction, whereas fault-slip inversion shows a horizontal compression in the WNW–ESE direction. In contrast, Kulmbach North (group 2) reveals the opposite trend, with stylolites recording WNW–ESE horizontal shortening, while fault-slip inversion suggests NNW–

SSE shortening. This stress field reactivated the Cretaceous strike-slip faults with a reverse slip sense, e.g. faults in the Eisfeld–Kulmbach FZ and in the Hersbruck FZ.

4.d. Oblique stress field

In addition to the main stress fields 1–5, our data indicate the existence of an oblique stress field, i.e. there is no vertical principal stress axis. Data separation for PBT analysis of group 2 (outcrop Kirchleus) led to a homogeneous cluster where σ_1 is oriented horizontally along the NE–SW direction, but neither σ_2 nor σ_3 is vertical (Fig. 12b). Figure 12a and c illustrate clusters of SF2- and SF-3 related data for the same outcrop. Bedding is (sub-)horizontal and σ_1 is parallel for all three stress fields, which differ only in the orientations of σ_2 and σ_3 .

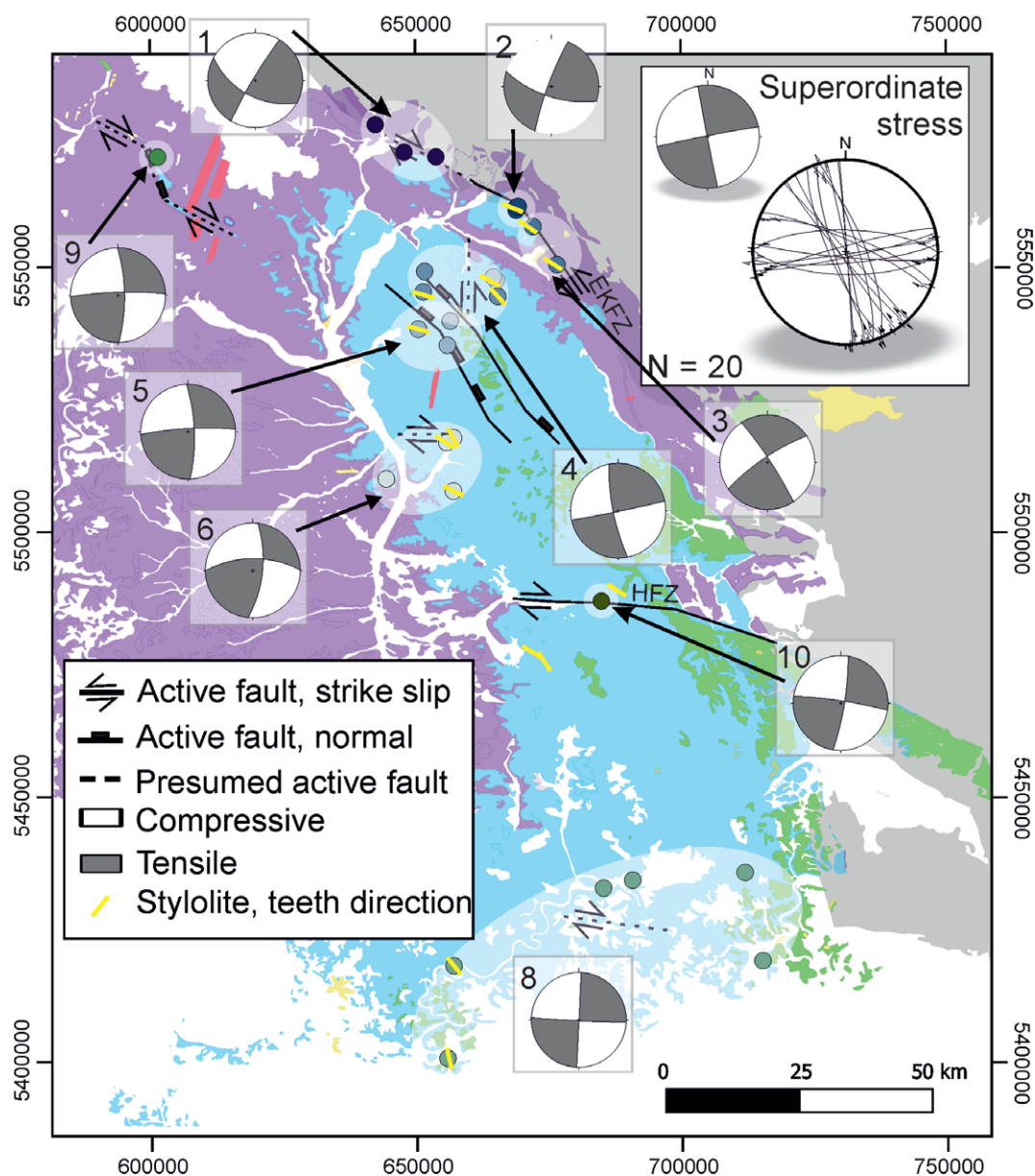


Fig. 11. Beachball plots illustrating regional variability of SF5 and prevailing NW–SE compression with NE–SW extension. Straight black lines show active, dashed lines probably active faults during SF5. Top right: beachball plot and stereographic projection (lower hemisphere) of SF5-related faults with slip sense. Teeth direction of tectonic stylolites is shown as yellow dashes. Abbreviations: EKFZ – Eisfeld–Kulmbach fault zone; HFZ – Hersbruck fault zone. See Figure 1 for key to colours and Table 1 for further details on outcrop groups.

5. Discussion

5.a. Timing of stress fields and correlation with over-regional structures on a Central European scale

5.a.1. Late Jurassic – Late Cretaceous NE–SW extension (SF1)

The oldest recorded stress field corresponds to a normal faulting regime with NE–SW-directed horizontal extension. The maximum age of this stress field is Late Jurassic due to the Malm stratigraphy of the youngest host rocks. The existence of a normal faulting regime prior to the Late Cretaceous inversion is in agreement with palaeostress results of other authors for the same area and adjacent regions (Bergerat & Geysant,

1982; Bergerat *et al.* 1992; Peterek *et al.* 1996, 1997). NE–SW-directed normal faulting is also recorded from Middle Triassic units in the adjacent Thuringian Basin (Navabpour *et al.* 2017). Because this stress field is no longer recorded in Upper Cretaceous sequences in the Elbe zone farther north (Coubal *et al.* 2015), its minimum age is Late Cretaceous. The timing of the stress field coincides with the tectonic evolution of the Central European Basin System (CEBS) that records sediment accumulation and subsidence from Late Permian to Late Cretaceous time (Scheck-Wenderoth *et al.* 2008; Stollhofen *et al.* 2008; von Eynatten *et al.* 2021). In the southern part of the CEBS, subsidence and extension have been related to the

Table 2. Orientation of SF1 and local deviations

Superordinate extension	σ_3 035/05	R% 90 %
Outcrop group	Dip direction σ_3 (horizontal) in degrees (°) towards north	Deviation (clockwise) in degrees (°)
5 Reef Facies	033	−2
6 Erlangen	228	13
8 Franconia South	052	17
9 Heldburg	224	9
10 Hersbruck	007	−28

Table 3. Orientation of SF2 and local deviations

Superordinate compression	σ_1 202/01	R% 97 %
Outcrop group	Dip direction σ_1 (horizontal) in degrees (°) towards north	Deviation (clockwise) in degrees (°)
2 Kulmbach North	019	−3
4 Central Franconia	024	2
6 Erlangen	206	4
10 Hersbruck	198	−4

reactivation of structures defining Permian NW–SE-striking basins (Zulauf & Duyster, 1997; Walter, 2007; Kley *et al.* 2008; Sippel *et al.* 2009; Navabpour *et al.* 2017).

5.a.2. Late Cretaceous NE–SW compressive phases (SF2 and SF3)

The folding and thrusting regime SF2 reactivated SF1-related structures. (N)NE–(S)SW-directed shortening is observed across the whole of western-central Europe (Kley & Voigt, 2008), and associated with lithospheric folding (e.g. Cloetingh & van Wees, 2005), inversion of Permian–Cretaceous basins and basement exhumation (Thomson & Zeh, 2000; von Eynatten *et al.* 2019, 2021). Based on stratigraphic and thermochronological constraints, the timing of this compressional phase is bracketed between *c.* 95 Ma and 75 Ma (Voigt *et al.* 2021). Viewed in a broader geodynamic context, the thrusting regime in western-central Europe is triggered by the onset of the convergence between Africa–Iberia–Europe (Kley & Voigt, 2008; Dielforder *et al.* 2019).

In our study area strike-slip faults cross-cut stylolites, faults and folds related to SF2. Thereby, the direction of maximum horizontal compression remains constant and the horizontal extension increases as shown by the change from a thrusting to a strike-slip regime under persisting orientation of σ_{Hmax} (Fig. 5). Thus, we assume that SF3 established shortly after SF2 and may represent the final stage of this compressional phase. This compressive phase started in the Franconian Platform with layer-parallel shortening and the development of tectonic stylolites, followed by folding and thrusting and eventually strike-slip faulting.

This chronological order is in agreement with palaeostress analysis from the Elbe Zone in the northeast (Coubal *et al.*

2015). There, volcanic dykes emplaced at 80–61 Ma (Ulrych *et al.* 2014) are related to a strike-slip regime postdating thrusting (Coubal *et al.* 2015). In the Thuringian Basin to the north, however, strike-slip faulting predates the thrusting regime (Navabpour *et al.* 2017), and in northern Germany the relative chronological order of the strike-slip and thrusting regime is not clearly resolved (Sippel *et al.* 2009).

5.a.3. Late Palaeogene – early Neogene NW–SE extension (SF4)

Stress field generation SF4 describes a normal faulting regime with σ_{hmin} trending NW–SE. This phase of extension with varying directions of σ_{hmin} is also recorded from the Thuringian Forest (E–W-directed extension; Rauche & Franzke, 1990); from the Thuringian Basin (WNW–ESE-directed extension; Navabpour *et al.* 2017); from the Bohemian Massif (WNW–ESE-directed extension; Coubal *et al.* 2015); from Northern Germany (radial extension, i.e. NW–SE- to NE–SW-directed; Sippel *et al.* 2009); from the Upper Rhine Graben (E–W-directed extension; Bergerat, 1987); and from the Lower Rhine Graben (NE–SW-directed extension; Vandycke, 2002). There are several interpretations of the reason for widespread intraplate extension and associated mafic volcanism in late Palaeogene to early Neogene time, such as asthenospheric melting in response to deeply rooted large-scale upwelling mantle plumes or small-scale diapiric upwelling (e.g. Hoernle *et al.* 1995; Wilson & Downes, 2006). There is, however, a temporal and genetic link to the onset of continental collisional tectonics, slab detachment and subsequent plate tectonic reconfigurations in the Alpine realm (e.g. Dèzes *et al.* 2004; Pfänder *et al.* 2018). Towards the south, normal faulting in the North Alpine Foreland Basin is interpreted to result from bulging, that is a consequence of the increasing thrust load of the Alpine Orogeny (von Hartmann *et al.* 2016).

As illustrated in Fig. 1a, the Franconian Platform records evidence of Cenozoic intraplate volcanism. A prominent example is the NNE–SSW-striking Heldburg dike swarm system. This system comprises two generations of dikes, the late Eocene to late Oligocene phase (38.0 Ma–25.4 Ma) and the Miocene phase (Abratis *et al.* 2007; Pfänder *et al.* 2018). Late Palaeogene – early Neogene intraplate volcanism is also evidenced by the 19–24 Ma Oberpfalz (Todt & Lippolt, 1975) and the ~31 Ma Oberleinleiter volcanism (Hofbauer, 2008; Fig. 1a). To the east of the Franconian fault zone even more pronounced extension-related volcanism is recorded from the NE–SW-striking Eger Graben which initially opened along a NNE–SSW to N–S direction during the late Eocene to latest Oligocene time, followed by NW–SE normal faulting during the early Miocene time (Adamovič & Coubal, 1999; Rajchl *et al.* 2009). Cenozoic intraplate volcanism was widespread in central Europe to the north of the Alpine front, e.g. the Upper Rhine Graben, Rhön, Vogelsberg (European Cenozoic Rift System; Dèzes *et al.* 2004). However, the high variability of the direction of σ_{hmin} over the whole of Europe cannot be explained exclusively by one cause. The strike direction of the Heldburg dike swarm differs from the direction of extension for SF4. On the other hand, a link to bulging as observed in the North Alpine Foreland Basin (*c.* 100 km farther south) requires additional consideration. Thus, the source for the normal faulting regime in the Franconian Platform remains unclear.

5.a.4. NW–SE-directed compressive phase since the Miocene time (SF5)

The youngest stress field is a strike-slip regime associated with NW–SE shortening. However, as compiled in Fig. 4 and stated

Table 4. Orientation of SF3 and local deviations

Superordinate strike-slip regime	σ_1 014/05	R% 98 %	σ_3 104/06	R% 95 %
Outcrop group	Dip direction σ_1 (horizontal) in degrees (°) towards north	Deviation (clockwise) in degrees (°)	Dip-direction σ_3 (horizontal) in degrees (°) towards north	Deviation (clockwise) in degrees (°)
1 Franconia North	221	27	128	24
2 Kulmbach North	012	−2	102	−2
4 Central Franconia	205	11	296	12
6 Erlangen	230	36	322	38
8 Franconia South	210	16	119	15
10 Hersbruck	239	45	329	45

Table 5. Orientation of SF4 and local deviations

Superordinate extension	137/01	R% 90 %
Outcrop group	Dip direction σ_3 (horizontal) in degrees (°) towards north	Deviation (clockwise) in degrees (°)
6 Erlangen	326	9
8 Franconia South	309	−8
9 Heldburg	302	−15
10 Hersbruck	147	10

in Section 4.a above, the relative chronology between SF4 and SF5 is not finally solved. SF5 is recorded by a high variability in the orientation of the active fault planes and in the orientation of stylolites.

This youngest compressional phase where bedding-parallel shortening (e.g. development of stylolites) and thrusting were subsequently replaced by an intracontinental strike-slip regime is also described for the whole of Central Europe (Rosenbaum *et al.* 2002; Kley & Voigt, 2008; Scheck-Wenderoth *et al.* 2008; Coubal *et al.* 2015; Navabpour *et al.* 2017). Kley and Voigt (2008) correlate this stress field with the Miocene to recent episode of the Alpine Orogeny and associated NW-directed shortening.

According to Heidbach *et al.* (2016) seismic activity and borehole break-outs imply the persistence of SF5 since the late Miocene time, because the respective stylolites are oriented parallel to the direction of σ_{Hmax} . We cannot exclude overlapping of stress fields 4 and 5. Figure 13 schematically illustrates the successive development from almost undeformed sedimentary rocks during SF1 (Fig. 13a) to a rather fractured upper crust recording the cumulative effects of SF1–5 deformations (Fig. 13e). Most probably fractures and stylolites led to mechanical anisotropies (Baud *et al.* 2016; Pfänder *et al.* 2018) and caused local deviation of plate collision induced stress.

5.b. Transitional stress fields

The stress field associated with NE–SW compression observed for Kirchleus (group 2, Franconian North; Section 4d above) is an exotic feature in our study area. Since there is no vertical principal stress axis, it represents a non-Andersonian behaviour (Anderson,

1972). Oblique stress fields could be the result of later, local tilting of preserved, older stress fields (SF2 or SF3) due to, e.g., folding or block rotation (Arboit *et al.* 2015; Navabpour *et al.* 2017). Tilting and folding, however, can be neglected due to the observation that the sedimentary layering is still horizontal.

Oblique stress fields can occur under upper crustal conditions as shown by recent studies (Lisle *et al.* 2006; Sippel *et al.* 2010; Lacombe, 2012; Beaudoin *et al.* 2016). For instance, if pre-existent structures or faults are not optimally oriented in the stress field, the reactivation leads to the partitioning of the stress tensor and/or the formation of oblique (transpressional or transtensional) fault kinematics (Sanderson & Marchini, 1984). Local perturbations are also promoted by the vicinity of fault zones (Homberg *et al.* 1997; Sippel *et al.* 2010; Lacombe, 2012; Beaudoin *et al.* 2016). In this case the outcrop might be affected by local stress deflection as it is located close to the EKFZ (e.g. Fig. 8).

There are three stress orientations with approximately the same orientation of σ_1 (= σ_{Hmax}) and (i) a vertical σ_3 (SF2, Fig. 12a), (ii) an oblique σ_2 and σ_3 (Fig. 12b) and (iii) a vertical σ_2 (SF3, Fig. 12c) recorded in the same outcrop. We therefore argue that this stress field (ii) most likely records a transitional stage between (i) and (iii), and thus between SF2 and SF3. This suggests that the stress field transition from thrusting to strike-slip is only locally preserved in Franconia. It is worth noting that the transition of stress fields, i.e. the change of the relative magnitudes of the principal stresses, may produce faulting in uniaxial stress geometries when the magnitudes of two principal stress axes become equal (Fig. 12e). The change in the magnitude of σ_v is supposed to be caused by thickening due to folding and thrusting (Dalmayrac & Molnar, 1981; Tavani *et al.* 2015; Ferrill *et al.* 2021). Thus, this observation can also represent snapshots of the oscillation between such different regimes during the transition as, e.g., shown by Beaudoin *et al.* (2016). The traces of the principal axis are shown in Fig. 12d.

5.c. Stress field consistency and perturbations

In some areas, e.g. Hersbruck (outcrop group 10), the orientation of local stress fields derived from fault-slip inversion deviates from that of the superordinate stress fields by up to 45° (Fig. 5; Tables 2–6). In those areas, however, the orientation of the maximum horizontal stress parallels the strike of large faults. For instance, σ_2 in SF1 and SF2 at locality Hersbruck (group 10) parallels the trace of the E–W-striking Hersbruck FZ, whereas at Kulmbach North (group 2) and Kulmbach South (group 3) σ_2 is oriented parallel to the NW–SE-striking Eisfeld–Kulmbach FZ (Figs 7, 8). In the strike-slip

Table 6. Orientation of SF5 and local deviations

Superordinate strike-slip regime	σ_1 124/04	R% 84 %	σ_3 214/03	R% 82 %
Outcrop group	Dip direction σ_1 (horizontal) in degrees (°) towards north	Deviation (clockwise) in degrees (°)	Dip direction σ_3 (horizontal) in degrees (°) towards north	Deviation (clockwise) in degrees (°)
1 Franconia North	325	21	064	30
2 Kulmbach North	347	43	81	47
4 Central Franconia	127	3	36	2
5 Reef Facies	320	16	226	12
6 Erlangen	132	8	218	4
8 Franconia South	322	18	225	11
9 Heldburg	304	0	211	-3

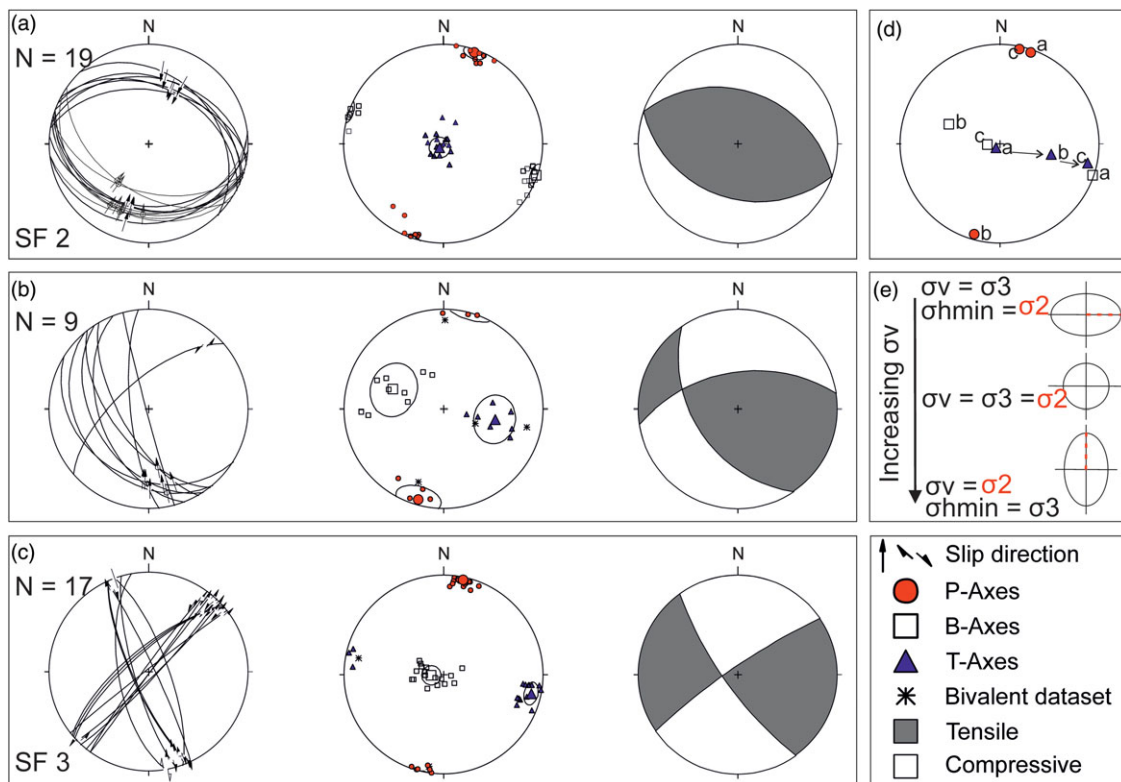


Fig. 12. Fault-slip measurements from locality Kirchleus (outcrop group 2), illustrating the proposed transition from (a) SF2, characterized by NNE-SSW compression with thrusting, over (b) transpression, to (c) SF3 with strike-slip faulting caused by NNE-SSW compression and WNW-ESE extension. For all stress fields the measured faults (stereographic projection, lower hemisphere), calculated PBT and the resulting beachball plot are provided. The bigger circles, squares and triangles show the mean orientation of P-, B- and T-axis, respectively. (d) shows the path of σ_3 from vertical orientation (a) to horizontal orientation (c). (e) Visualization of the of the σ_2 - σ_3 stress ellipse (in a vertical plane) with changing orientation due to increasing σ_v . The increase in σ_v changes the orientation of σ_2 changes from horizontal (a, top, SF2) to vertical (c, bottom, SF3). The σ_2 axis of the stress ellipse is shown as a dashed line.

regimes of SF3 and SF5 the respective large faults are reactivated. SF3 reactivates the Hersbruck FZ in a sinistral sense of movement and the Eisfeld-Kulmbach FZ in a dextral sense of movement and vice versa for SF5. Another possible explanation for the difference in the stress orientation could be that the area of outcrop group 10 is located in the region of potential interaction between the tips of the PSZ and a minor fault parallel to the NNW-SSE-striking PSZ. According to Homberg *et al.* (1997, 2004), stress perturbation near fault tips is significantly influenced by the respective fault and the magnitude of the applied stresses. The coincidence of the orientation

of σ_2 and the strike of nearby faults indicates that stress deflection due to the existence of structural heterogeneities (*sensu* Hudson & Cooling, 1988; Casas *et al.* 1992; Zhang *et al.* 1994; Bell, 1996; de Jossineau *et al.* 2003; Yale, 2003) plays a significant role in the Franconian Platform.

However, the overall stress field is relatively constant. This leads to the validation of assumption 2, made in Section 3 above, the negligibility of block rotation. If perturbations may be induced by block rotation palaeostress studies need to be conducted in the area to the south in order to obtain a larger framework.

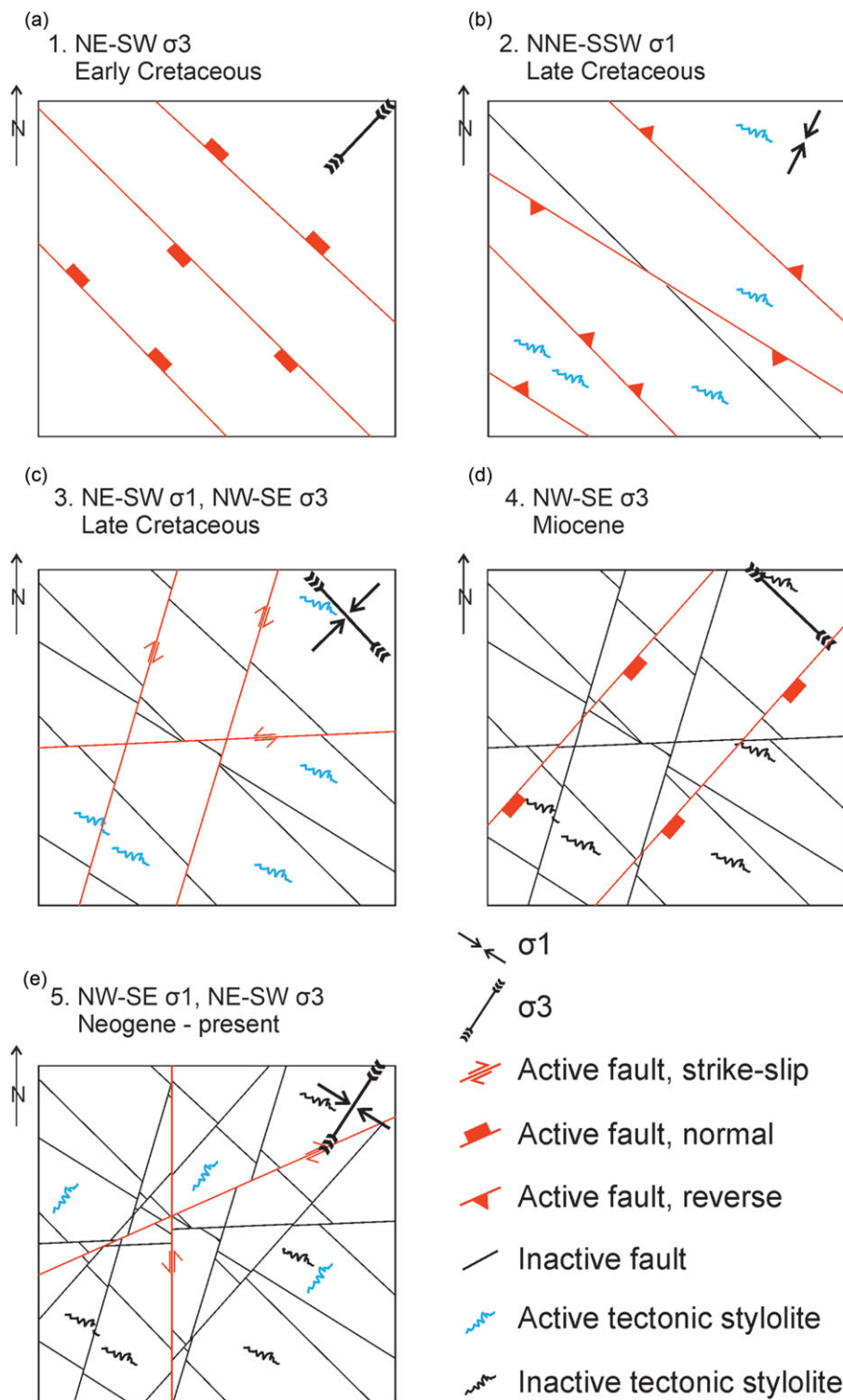


Fig. 13. Summary sketch (map view) illustrating the development of faults and tectonic stylolites during stress fields 1–5. (a) SF1: normal faulting regime with σ_{hmin} trending NE-SW; (b) SF2: thrusting regime with σ_{hmax} trending NNE-SSW; (c) SF3: strike-slip regime with σ_{hmax} trending NE-SW; (d) SF4: normal faulting regime with σ_{hmin} trending NW-SE; (e) SF5: strike-slip regime with σ_{hmax} trending NW-SE.

5.d. Cyclic stress fields in compressional regimes

Our stress inversion results from the Franconian Platform can be explained in the frame of fold-and-thrust belt cycles *sensu* Tavani *et al.* (2015) and Ferrill *et al.* (2021). For instance, SF1–SF3 represent a complete cycle, initiated by normal faulting due to fault-controlled subsidence, followed by the formation of tectonic stylolites and basin inversion by folding and thrusting. Due to the

resulting thickness of the crust during SF2, the vertical stress increases while the orientation of σ_{Hmax} persists (Fig. 12e). Assuming that the magnitude of σ_1 (σ_{Hmax}) also remained, the exclusive increase of the vertical stress would cause the differential stress to decrease. Since the differential stress needs to be large enough to produce faulting, this scenario would interrupt the brittle deformation (Coulomb, 1776; Mohr, 1900). Strike-slip faulting

during SF3 requires the accommodation of faulting exclusively by reactivation of pre-existing faults or fluid overpressure that reduced the mean stress. There is, however, no evidence for both the exclusive reactivation of pre-existing faults and the presence of fluids (e.g. low-T mineralization). Another scenario with fault-parallel, i.e. NW–SE directed, horizontal extension would allow maintaining the differential stress by reducing σ_{hmin} to approach σ_3 during an increase of σ_v to approach σ_2 . Nevertheless, this remains an open question since there is (yet) no record for related structures nor have we obtained absolute or relative magnitudes of stresses. An increase of σ_1 after the main compressional phase (SF2), however, is in disagreement with the weakened coupling between Iberia and Europe after the collision (Dielforder *et al.* 2019).

This final phase of the tectonic cycle is characterized by the switch of the fault regimes from thrusting to strike-slip and eventually normal faulting (Dalmayrac & Molnar, 1981; Molnar & Chen, 1983). A pause between thrusting and strike-slip faulting probably provides time for another set of tectonic stylolites to grow. A similar chronology containing normal faulting, thrusting, folding and strike-slip faulting is described for the Indochina block in Thailand (Arboit *et al.* 2015). There, deformation started with extension replaced by layer-parallel shortening in the same direction. Features produced by this compression (stylolites, pressure-solution cleavage) were rotated by folding afterwards.

The detailed analysis of the stylolites to determine the exact orientation of the in-plane principal stresses (σ_2 and σ_3) (Ebner *et al.* 2010) is not within the scope of this work. Thus, we cannot distinguish if the stylolites developed in SF2 or before in another strike-slip regime. Both options are in agreement with the concept of Ferrill *et al.* (2021). The observation of a younger strike-slip regime (SF3) cross-cutting faults and folds of SF2 challenges the concept by Tavani *et al.* (2015), where no late strike-slip regime is included. In addition, this concept is simplified with respect to stylolites which are assumed to develop in strike-slip regimes, exclusively. This makes a fundamental difference in the stress evolution in the foreland area. However, the switch from thrusting to strike-slip regime is also described for the western Alpine foreland (Smeraglia *et al.* 2021). The earlier extension is not observed there.

An incipient second stress cycle is documented by a second generation of tectonic stylolites. The apparent coexistence of strike-slip faulting, however, does not allow us to infer the relative-chronological order of the stress fields within the new stress cycle. The strike-slip faults can either result from early compression or initial relaxation, or both. The latter case would imply the existence of two generations of strike-slip faults which we cannot distinguish here. Regarding the heterogeneous directions of Late Palaeogene to Neogene normal faulting and the fact that the extension is sub-parallel to the younger compression SF5 (see Section 5.a.3 above) the tectonic cause of SF4 remains unclear. If the extension is linked to foreland bulging induced by the Alpine collision, this stress field SF4 could represent an earlier extensional episode prior to shortening.

6. Conclusion

We use fault slip analysis and tectonic stylolites to reproduce a highly resolved stress evolution of the Franconian Platform in SE Germany. The analysis allows us to reconstruct the complete tectonic cycle of an inverted basin that originated from initial Late Jurassic – Early Cretaceous extension and subsidence (SF1), followed by successive NE–SW-directed shortening through

layer-parallel shortening and the growth of tectonic stylolites and later thrusting and folding (SF2), and a final Late Cretaceous relaxation (SF3). The inversion cycle becomes repeated during a second phase of extension (SF4) and shortening in NW–SE direction (SF5) with a second set of tectonic stylolites and strike-slip to oblique slip faults. During these stress cycles, the main principal stresses switch systematically from Andersonian extensional regime to thrusting, strike-slip and extensional again. The transitions are sometimes preserved in oblique stress fields, with σ_1 being the only principal stress in the horizontal plane. Pre-existing faults seem to partly account for small-scale perturbations. Our study provides a crucial insight into the stress development in an intraplate compressional setting where two inversion events developed with their highest horizontal stresses in nearly perpendicular orientation to each other: the first during the Africa–Iberia–Europe convergence followed by a period of extension and then the development of the Alpine orogeny.

Acknowledgements. The authors thank for the comments by the guest editors Olivier Lacombe and Stefano Tavani, and by Jonas Kley and an anonymous reviewer that helped to improve the manuscript.

This research is funded by the project ‘Integrated geophysical–structural–kinematic analysis of the fault patterns in Northern Bavaria’ within the scope of ‘Bodenatlas Bayern’ by the Bayerisches Landesamt für Umwelt (LfU) and the European Union (ERDF program Bayern 2014–2020) which is gratefully acknowledged. Many thanks to T. Voigt for motivating discussions and precious outcrop suggestions.

Conflict of interest. None.

References

- Abratis M, Mädler J, Hautmann S, Leyk H-J, Meyer R, Lippolt HJ and Viereck-Götte L (2007) Two distinct Miocene age ranges of basaltic rocks from the Rhön and Heldburg areas (Germany) based on $^{40}\text{Ar}/^{39}\text{Ar}$ step heating data. *Geochemistry* **67**, 133–50.
- Adamovič J and Coubal M (1999) Intrusive geometries and Cenozoic stress history of the northern part of the Bohemian Massif. *Geolines* **9**, 5–14.
- Anderson EM (1972) *The Dynamics of Faulting and Dyke Formation with Applications to Britain*. New York: Hafner Publishing Comp.
- Angelier J (1984) Tectonic analysis of fault slip data sets. *Journal of Geophysical Research* **89**, 5835–48.
- Arboit F, Amrouch K, Collins AS, King R and Morley C (2015) Determination of the tectonic evolution from fractures, faults, and calcite twins on the southwestern margin of the Indochina Block. *Tectonics* **34**, 1576–99.
- Baud P, Rolland A, Heap M, Xu T, Nicolé M, Ferrand T, Reuschlé T, Toussaint R and Conil N (2016) Impact of stylolites on the mechanical strength of limestone. *Tectonophysics* **690**, 4–20.
- Beaudoin N, Koehn D, Lacombe O, Lecouty A, Billi A, Aharonov E and Parlangeau C (2016) Fingerprinting stress: stylolite and calcite twinning paleopiezometry revealing the complexity of progressive stress patterns during folding: the case of the Monte Nero anticline in the Apennines, Italy. *Tectonics* **35**, 1687–712.
- Beaudoin N and Lacombe O (2018) Recent and future trends in paleopiezometry in the diagenetic domain: insights into the tectonic paleostress and burial depth history of fold-and-thrust belts and sedimentary basins. *Journal of Structural Geology* **114**, 357–65.
- Bell JS (1996) Petro Geoscience 2. In situ stresses in sedimentary rocks (part 2): applications of stress measurements. *Geoscience Canada* **23**.
- Bergerat F (1987) Stress fields in the European platform at the time of Africa–Eurasia collision. *Tectonics* **6**, 99–132.
- Bergerat F, Bouroz-Weil C and Angelier J (1992) Palaeostresses inferred from macrofractures, Colorado Plateau, western U.S.A. *Tectonophysics* **206**, 219–43.

- Bergerat F and Geysant J** (1982) Tectonique cassante et champ de contraintes tertiaire en avant des Alpes orientales: le Jura souabe. *Geologische Rundschau* **71**, 537–48.
- Blés JL, Bonijoly D, Castaing C and Gros Y** (1989) Successive post-Variscan stress fields in the French Massif Central and its borders (Western European plate): comparison with geodynamic data. *Tectonophysics* **169**, 79–111.
- Büttner SH** (2012) Late Variscan stress-field rotation initiating escape tectonics in the south-western Bohemian Massif: a far field response to late-orogenic extension. *Journal of Geosciences* **52**, 29–43.
- Casas AM, Simon JL and Seron FJ** (1992) Stress deflection in a tectonic compressional field: a model for the northwestern Iberian Chain, Spain. *Journal of Geophysical Research* **97**, 7183.
- Cloetingh S and van Wees JD** (2005) Strength reversal in Europe's intraplate lithosphere: transition from basin inversion to lithospheric folding. *Geology* **33**, 285–88.
- Coubal M, Málek J, Adamovič J and Štěpančíková P** (2015) Late Cretaceous and Cenozoic dynamics of the Bohemian Massif inferred from the paleostress history of the Lusatian Fault Belt. *Journal of Geodynamics* **87**, 26–49.
- Coulomb CA** (1776) Essai sur une application des règles des maximis et minimis à quelques problèmes de statique relatifs à l'architecture. *Mémoires Académie Royale Présentés par Divers Savants* **7**, 343–82.
- Dalmayrac B and Molnar P** (1981) Parallel thrust and normal faulting in Peru and constraints on the state of stress. *Earth and Planetary Science Letters* **55**, 473–81.
- de Jossineau G, Petit J-P and Gauthier BDM** (2003) Photoelastic and numerical investigation of stress distributions around fault models under biaxial compressive loading conditions. *Tectonophysics* **363**, 19–43.
- Dèzes P, Schmid SM and Ziegler PA** (2004) Evolution of the European Cenozoic Rift System: interaction of the Alpine and Pyrenean orogens with their foreland lithosphere. *Tectonophysics* **389**, 1–33.
- Dielforder A, Frasca G, Brune S and Ford M** (2019) Formation of the Iberian-European convergent plate boundary fault and its effect on intraplate deformation in Central Europe. *Geochemistry, Geophysics, Geosystems* **102**, 22–497.
- Digitale Geologische Karte von Bayern 1:25 000** (2020) Bayerisches Landesamt für Umwelt. Online Supplementary Material at https://www.lfu.bayern.de/geologie/geo_karten_schriften/dgk25_uab/index.htm (accessed 22 April 2022).
- Ebner M, Toussaint R, Schmittbuhl J, Koehn D and Bons P** (2010) Anisotropic scaling of tectonic stylolites: a fossilized signature of the stress field? *Journal of Geophysical Research* **115**, 1–16. doi: [10.1029/2009JB006649](https://doi.org/10.1029/2009JB006649)
- Fazlikhani H, Bauer W and Stollhofen H** (2022) Variscan structures and their control on latest to post-Variscan basin architecture; insights from the westernmost Bohemian Massif and southeastern Germany. *Solid Earth* **13**, 393–416.
- Ferrill DA, Smart KJ, Cawood AJ and Morris AP** (2021) The fold-thrust belt stress cycle: superposition of normal, strike-slip, and thrust faulting deformation regimes. *Journal of Structural Geology* **148**, 104362.
- Freudenberger W and Schwerd K** (1996) *Erläuterungen zur Geologischen Karte von Bayern 1:500000*, 340 pp. Bayerisches Geologisches Landesamt.
- Glottbach C, Reinecker J, Danišik M, Rahn M, Frisch W and Spiegel C** (2010) Thermal history of the central Gotthard and Aar massifs, European Alps: evidence for steady state, long-term exhumation. *Journal of Geophysical Research* **115**, F03017.
- Heidbach O, Rajabi M, Reiter K, Ziegler M and WSM Team** (2016) *World Stress Map Database Release 2016*. GFZ Data Services. Online Supplementary Material at <http://dataservices.gfz-potsdam.de/wsm/showshort.php?id=escidoc:1680890>.
- Heinicke J, Stephan T, Alexandrakis C, Gaupp R and Buske S** (2019) Alteration as possible cause for transition from brittle failure to aseismic slip: the case of the NW-Bohemia/Vogtland earthquake swarm region. *Journal of Geodynamics* **124**, 79–92.
- Hejl E, Coyle D, Lal N, van den Haute P and Wagner GA** (1997) Fission-track dating of the western border of the Bohemian Massif: thermochronology and tectonic implications. *Geologische Rundschau* **86**, 210–19.
- Hibsch C, Jarrige J-J, Cushing EM and Mercier J** (1995) Palaeostress analysis, a contribution to the understanding of basin tectonics and geodynamic evolution. Example of the Permian/Cenozoic tectonics of Great Britain and geodynamic implications in western Europe. *Tectonophysics* **252**, 103–36.
- Hoernle K, Zhang Y-S and Graham D** (1995) Seismic and geochemical evidence for large-scale mantle upwelling beneath the eastern Atlantic and western and central Europe. *Nature* **374**, 34–39.
- Hofbauer G** (2008) Der Vulkan von Oberleinleiter: Zeugnisse eines Maars in der Nördlichen Frankenalb. *Natur und Mensch, Jahresmitteilungen*, 2008.
- Homberg C, Angelier J, Bergerat F and Lacombe O** (2004) Using stress deflections to identify slip events in fault systems. *Earth and Planetary Science Letters* **217**, 409–24.
- Homberg C, Hu JC, Angelier J, Bergerat F and Lacombe O** (1997) Characterization of stress perturbations near major fault zones: insights from 2-D distinct-element numerical modelling and field studies (Jura mountains). *Journal of Structural Geology* **19**, 703–18.
- Hudson JA and Cooling CM** (1988) In situ rock stresses and their measurement in the U.K. – Part I. The current state of knowledge. *International Journal of Rock Mechanics and Mining Science & Geomechanics Abstracts* **25**, 356–70.
- Kämmlein M, Bauer W and Stollhofen H** (2020) The Franconian Basin thermal anomaly, SE Germany revised: new thermal conductivity and uniformly corrected temperature data. *Zeitschrift der Deutschen Gesellschaft für Geowissenschaften* **171**, 21–44.
- Kley J, Franzke H-J, Jähne F, Krawczyk C, Lohr T, Reicherter K, Scheck-Wenderoth M, Sippel J, Tanner DC and van Gent H** (2008) Strain and stress. In *Dynamics of Complex Intracontinental Basins: The Central European Basin System* (eds R Littke, U Bayer, D Gajewski and S Nelskamp). Berlin: Springer Science & Business Media.
- Kley J and Voigt T** (2008) Late Cretaceous intraplate thrusting in central Europe: effect of Africa-Iberia-Europe convergence, not Alpine collision. *Geology* **36**, 839–42.
- Koehn D, Ebner M, Renard F, Toussaint R and Passchier CW** (2012) Modelling of stylolite geometries and stress scaling. *Earth and Planetary Science Letters* **341–344**, 104–13.
- Koehn D, Renard F, Toussaint R and Passchier CW** (2007) Growth of stylolite teeth patterns depending on normal stress and finite compaction. *Earth and Planetary Science Letters* **257**, 582–95.
- Köhler S, Bücker J, Hofmann N and Koehn D** (2021) Field measurements of fault planes, slip direction, tectonic stylolites, joints and bedding in Mesozoic rocks in Northern Bavaria (Germany). doi: [10.1594/PANGAEA.929490](https://doi.org/10.1594/PANGAEA.929490).
- Kossmat F** (1927) *Gliederung des varistischen Gebirgsbaues*. Abhandlungen Sächsisches Geologisches Landes-Amt. Leipzig and Dresden: G. A. Kaufmann's Buchhandlung.
- Kroner U, Hahn T, Romer RL and Linnemann U** (2007) The Variscan Orogeny in the Saxo-Thuringian zone: heterogeneous overprint of Cadomian/Paleozoic Peri-Gondwana crust. In *The Evolution of the Rheic Ocean: From Avalonian-Cadomian Active Margin to Alleghenian-Variscan Collision* (eds U Linnemann, RD Nance, P Kraft and G Zulauf), pp. 153–72. Geological Society of America, Special Paper no. 423. Online Supplementary Material at <http://specialpapers.gsapubs.org/content/423/153>.
- Kroner U and Romer RL** (2013) Two plates – many subduction zones: the Variscan orogeny reconsidered. *Gondwana Research* **24**, 298–329.
- Lacombe O** (2012) Do fault slip data inversions actually yield “paleostresses” that can be compared with contemporary stresses? A critical discussion. *Comptes Rendus Geoscience* **344**, 159–73.
- Lisle RJ** (2013) A critical look at the Wallace-Bott hypothesis in fault-slip analysis. *Bulletin de la Société Géologique de France* **184**, 299–306.
- Lisle RJ, Orifé TO, Arlegui L, Liesa C and Srivastava DC** (2006) Favoured states of palaeostress in the earth's crust: evidence from fault-slip data. *Journal of Structural Geology* **28**, 1051–66.
- Meyer RKF and Schmidt-Kaler H** (1990) Paläogeographie und Schwammriffentwicklung des süddeutschen Malm – ein Überblick. *Facies* **23**, 175–84.
- Mohr O** (1900) Welche Umstände bedingen die Elastizitätsgrenze und den Bruch eines Materials? *Zeitschrift des Vereins deutscher Ingenieure* **1524–1530**, 1572–7.

- Molnar P and Chen W-P** (1983) Focal depths and fault plane solutions of earthquakes under the Tibetan Plateau. *Journal of Geophysical Research* **88**, 1180–96.
- Munk C** (1980) Foraminiferen aus dem unteren Kimmeridge (Platynota-Schichten) der Nördlichen und Mittleren Frankenalb – Faunenbestand und Palökologie. *Facies* **2**, 149–217.
- Navabpour P, Malz A, Kley J, Sieburg M, Kasch N and Ustaszewski K** (2017) Intraplate brittle deformation and states of paleostress constrained by fault kinematics in the central German platform. *Tectonophysics* **694**, 146–63.
- Niebuhr B, Wilmsen M and Janetschke N** (2014) Cenomanian-Turonian sequence stratigraphy and facies development of the Danubian Cretaceous Group (Bavaria, Southern Germany). *Zeitschrift der Deutschen Gesellschaft für Geowissenschaften* **165**, 621–40.
- Nitecki MH** (1962) Observations on Slickolites. *SEPM Journal of Sedimentary Research* **32**, 435–9.
- Ortner H, Reiter F and Acs P** (2002) Easy handling of tectonic data: the programs TectonicVB for Mac and TectonicsFP for Windows™. *Computers & Geosciences* **28**, 1193–200.
- Park WC and Schot EH** (1968) Stylolites: their nature and origin. *Journal of Sedimentary Petrology* **38**, 175–91.
- Paul J and Schröder B** (2012) Rotliegend im Ostteil der Süddeutschen Scholle. *Schriftenreihe der Deutschen Gesellschaft für Geowissenschaften* **61**, 697–706.
- Petek A, Rauche H and Schröder B** (1996) Die strukturelle Entwicklung des E-Randes der Süddeutschen Scholle in der Kreide. *Zeitschrift für Geologische Wissenschaften* **24**, 65–77.
- Petek A, Rauche H, Schröder B, Franzke H-J, Bankwitz P and Bankwitz E** (1997) The late-and post-Variscan tectonic evolution of the Western Border fault zone of the Bohemian massif (WBZ). *Geologische Rundschau* **86**, 191–202.
- Pfänder JA, Jung S, Klügel A, Münker C, Romer RL, Sperner B and Rohrmüller J** (2018) Recurrent local melting of metasomatised lithospheric mantle in response to continental rifting: constraints from basanites and nephelinites/melilitites from SE Germany. *Journal of Petrology* **59**, 667–94.
- Rajchl M, Uličný D, Grygar R and Mach K** (2009) Evolution of basin architecture in an incipient continental rift: the Cenozoic Most Basin, Eger Graben (Central Europe). *Basin Research* **21**, 269–94.
- Rauche H and Franzke H-J** (1990) Stress field evolution at the northern part of the South German Block of the territory of the GDR. *Gerlands Beiträge zur Geophysik* **99**, 441–61.
- Reicherter K, Froitzheim N, Jarosinski M, Badura J, Franzke H-J, Hansen M, Hübscher C, Müller R, Poprawa P, Reinecker J, Stackebrandt W, Voigt T, von Eynatten H and Zuchiewicz W** (2008) Alpine Tectonics II – Central Europe north of the Alps. In *The Geology of Central Europe: Volume 2: Mesozoic and Cenozoic* (ed T McCann), pp. 1233–85. London: The Geological Society.
- Reiter F and Acs P** (2020) *Tectonics FP: Software for Structural Geology*. Online Supplementary Material at <http://www.tectonicsfp.com> (accessed 15 June 2020).
- Röckel T and Wonik T** (2006) Strukturauswertungen von Bohrlochmessungen der Forschungsbohrung Lindau 1 (Bayreuth). *Geologica Bavarica* **109**, 151–83.
- Rosenbaum G, Lister GS and Duboz C** (2002) Relative motions of Africa, Iberia and Europe during Alpine Orogeny. *Tectonophysics* **359**, 117–29.
- Sanderson DJ and Marchini WRD** (1984) Transpression. *Journal of Structural Geology* **6**, 449–58.
- Scheck-Wenderoth M, Krzywiec P, Zühlke R, Maystrenko Y and Froitzheim N** (2008) Permian to Cretaceous tectonics. In *The Geology of Central Europe: Volume 2: Mesozoic and Cenozoic* (ed T McCann), pp. 999–1030. London: The Geological Society.
- Schmittbuhl J, Renard F, Gratier JP and Toussaint R** (2004) Roughness of stylolites: implications of 3D high resolution topography measurements. *Physical Review Letters* **93**, 238501.
- Schröder B** (1987) Inversion tectonics along the western margin of the Bohemian Massif. *Tectonophysics* **137**, 93–100.
- Schröder B, Ahrendt H, Peterek A and Wemmer K** (1997) Post-Variscan sedimentary record of the SW margin of the Bohemian massif: a review. *Geologische Rundschau* **86**, 178–84.
- Sippel J, Saintot A, Heeremans M and Scheck-Wenderoth M** (2010) Paleostress field reconstruction in the Oslo region. *Marine and Petroleum Geology* **27**, 682–708.
- Sippel J, Scheck-Wenderoth M, Reicherter K and Mazur S** (2009) Paleostress states at the south-western margin of the Central European Basin System: application of fault-slip analysis to unravel a polyphase deformation pattern. *Tectonophysics* **470**, 129–46.
- Sittig E** (2012) Stefan und Rotliegend zwischen Odenwald und Alpenrand. *Schriftenreihe der Deutschen Gesellschaft für Geowissenschaften* **61**, 646–96.
- Smeraglia L, Looser N, Fabbri O, Choulet F, Guillong M and Bernasconi SM** (2021) U–Pb dating of middle Eocene–Pliocene multiple tectonic pulses in the Alpine foreland. *Solid Earth* **12**, 2539–51.
- Sperner B and Zweigel P** (2010) A plea for more caution in fault–slip analysis. *Tectonophysics* **482**, 29–41.
- Stephan T, Kroner U, Hahn T, Hallas P and Heuse T** (2016) Fold/cleavage relationships as indicator for late Variscan sinistral transpression at the Rheno-Hercynian–Saxo-Thuringian boundary zone, Central European Variscides. *Tectonophysics* **681**, 250–62.
- Stollhofen H, Bachmann GH, Barnasch J, Bayer U, Beutler G, Franz M, Kästner M, Legler B, Mutterlose J and Radies D** (2008) Upper Rotliegend to early Cretaceous basin development. In *Dynamics of Complex Intracontinental Basins: The Central European Basin System* (eds R Littke, U Bayer, D Gajewski and S Nelskamp), pp. 181–210. Berlin: Springer Science & Business Media.
- Stübner K, Ratschbacher L, Rutte D, Stanek K, Minaev V, Wiesinger M and Gloaguen R** (2013) The giant Shakh-dara migmatitic gneiss dome, Pamir, India-Asia collision zone: 1. Geometry and kinematics. *Tectonics* **32**, 948–79.
- Tanner DC, Behrmann JH, Oncken O and Weber K** (1998) Three-dimensional retro-modelling of transpression on a linked fault system: the Upper Cretaceous deformation on the western border of the Bohemian Massif, Germany. In *Continental Transpressional and Transtensional Tectonics* (eds RE Holdsworth, RA Strachan and JF Dewey), pp. 275–87. *Geological Society of London, Special Publications* no. 135.
- Tavani S, Storti F, Lacombe O, Corradetti A, Muñoz JA and Mazzoli S** (2015) A review of deformation pattern templates in foreland basin systems and fold-and-thrust belts: implications for the state of stress in the frontal regions of thrust wedges. *Earth-Science Reviews* **141**, 82–104.
- Thomson SN and Zeh A** (2000) Fission-track thermochronology of the Ruhla Crystalline Complex: new constraints on the post-Variscan thermal evolution of the NW Saxo-Bohemian Massif. *Tectonophysics* **324**, 17–35.
- Todt W and Lippolt HJ** (1975) K-Ar-Altersbestimmung an Vulkaniten bekannter paläomagnetischer Feldrichtung. I. Oberpfalz und Oberfranken. *Journal of Geophysics* **41**, 43–61.
- Toussaint R, Aharonov E, Koehn D, Gratier J-P, Ebner M, Baud P, Rolland A and Renard F** (2018) Stylolites: a review. *Journal of Structural Geology* **114**, 163–95.
- Turner FJ** (1953) Nature and dynamic interpretation of deformation lamellae in calcite of three marbles. *American Journal of Science* **251**, 276–98.
- Twiss RJ and Moores EM** (1992) *Structural Geology*. San Francisco: W. H. Freeman & Co.
- Ulrych J, Adamović J, Krmíček L, Ackerman L and Balogh K** (2014) Revision of Scheumann's classification of melilitic lamprophyres and related melilitic rocks in light of new analytical data. *Journal of Geosciences* **59**, 3–22.
- van der Pluijm BA, Craddock JP, Graham BR and Harris JH** (1997) Paleostress in cratonic North America: implications for deformation of continental interiors. *Science* **277**, 794–6.
- Vandycke S** (2002) Paleostress records in Cretaceous formations in NW Europe: extensional and strike-slip events in relationships with Cretaceous-Tertiary inversion tectonics. *Tectonophysics* **357**, 119–36.
- Voigt T, Kley J and Voigt S** (2021) Dawn and dusk of Late Cretaceous basin inversion in central Europe. *Solid Earth* **12**, 1443–71.
- von Eynatten H, Dunkl I, Brix M, Hoffmann V-E, Raab M, Thomson SN and Kohn B** (2019) Late Cretaceous exhumation and uplift of the Harz Mountains, Germany: a multi-method thermochronological approach. *International Journal of Earth Sciences* **108**, 2097–111.
- von Eynatten H, Kley J, Dunkl I, Hoffmann V-E and Simon A** (2021) Late Cretaceous to Paleogene exhumation in central Europe: localized inversion vs. large-scale domal uplift. *Solid Earth* **12**, 935–58.

- von Hartmann H, Tanner DC and Schumacher S** (2016) Initiation and development of normal faults within the German alpine foreland basin: the inconspicuous role of basement structures. *Tectonics* **35**, 1560–74.
- Wallbrecher E** (1986) *Tektonische und gefügearalytische Arbeitsweisen: Graphische, rechnerische und statistische Verfahren*. Stuttgart: Ferdinand Enke Verlag.
- Walter R** (2007) *Geologie von Mitteleuropa*. Stuttgart: Schweizerbart, 511 pp.
- Wilde-Piórko M, Geissler WH, Plomerová J, Knapmeyer-Endrun B, Grad M, Babuška V, Brückl E, Cyziene J, Czuba W, England R, Gaczyński E, Gazdova R, Gregersen S, Guterch A, Hanka W, Hegedús E, Heuer B, Jedlička P, Lazauskiene J, Keller GR, Kind R, Klinge K, Kolinsky P, Komminaho K, Kozlovskaya E, Krüger F, Larsen T, Majdański M, Malek J, Motuza G, Novotný O, Pietrasiak R, Plenefisch T, Růžek B, Sliapa S, Šroda P, Świeczak M, Tiira T, Voss P and Wiejacz P** (2006) Pässeq 2006–2008: passive seismic experiment in trans-European suture zone. GFZ Data Services. Other/Seismic Network. doi: [10.14470/2R383989](https://doi.org/10.14470/2R383989)
- Wilson M and Downes H** (2006) Tertiary-Quaternary intra-plate magmatism in Europe and its relationship to mantle dynamics. In *European Lithosphere Dynamics* (eds DG Gee & RA Stephenson), pp. 147–66. *Geological Society of London, Memoirs* **32**.
- Yale DP** (2003) Fault and stress magnitude controls on variations in the orientation of in situ stress. In *Fracture and in-situ Stress Characterization of Hydrocarbon Reservoirs* (ed. M. Ameen), pp. 55–64. *Geological Society of London, Special Publication* no. 209.
- Zhang Y-Z, Dusseault MB and Yassir NA** (1994) Effects of rock anisotropy and heterogeneity on stress distributions at selected sites in North America. *Engineering Geology* **37**, 181–97.
- Ziegler PA** (1992) European Cenozoic rift system. *Tectonophysics* **208**, 91–111.
- Ziegler PA, Cloetingh S and van Wees J-D** (1995) Dynamics of intra-plate compressional deformation: the Alpine foreland and other examples. *Tectonophysics* **252**, 7–59.
- Zoback ML and Zoback MD** (1989) *Chapter 24: Tectonic Stress Field of the Continental United States*. Online Supplementary Material at <https://pubs.geoscienceworld.org/gsa/books/book/173/chapter/3793042/chapter-24-tectonic-stress-field-of-the>.
- Zulauf G and Duyster J** (1997) Faults and veins in the superdeep well KTB: constraints on the amount of Alpine intra-plate thrusting and stacking of Variscan basement (Bohemian Massif, Germany). *Geologische Rundschau* **86**, S28–S33.